N^6-methyladenosine RNA modification regulates strawberry fruit ripening in an ABA-dependent manner

Leilei Zhou[1,2,#], Renkun Tang[1,2,#], Xiaojing Li[1,2], Shiping Tian[1,2], Bingbing Li[3], Guozheng Qin[1,2*]

[1]Key Laboratory of Plant Resources, Institute of Botany, Innovation Academy for Seed Design, Chinese Academy of Sciences, No.20 Nanxincun, Xiangshan, Haidian District, Beijing 100093, China.

[2]University of Chinese Academy of Sciences, Beijing 100049, China.

[3]College of Horticulture, China Agricultural University, Beijing 100193, China.

[#]These authors contributed equally

[*]Correspondence: gzqin@ibcas.ac.cn

Abstract

Background: Epigenetic marks, such as DNA methylation, play pivotal roles in regulating ripening of both climacteric and non-climacteric fruits. However, it remains unclear whether mRNA m^6A methylation, the epitranscriptome, is functionally conserved for ripening control.

Results: Here we show that m^6A methylation, which has been revealed to regulate ripening of tomato, a typical climacteric fruit, displays a dramatic change at ripening onset of strawberry, a classical non-climacteric fruit. The m^6A modification in the coding sequence (CDS) regions appears to be ripening-specific and tends to stabilize the mRNAs, whereas m^6A around the stop codons and within the 3' untranslated regions is generally negatively correlated with the abundance of the mRNAs. We identified thousands of transcripts with m^6A hypermethylation in the CDS regions, including those of *NCED5*, *ABAR*, and *AREB1* in the abscisic acid (ABA) biosynthesis and signaling pathway. We demonstrated that the methyltransferases MTA and MTB are indispensable for normal ripening of strawberry fruit, and MTA-mediated m^6A modification promotes mRNA stability of *NCED5* and *AREB1*, while facilitates translation of *ABAR*.

Conclusion: Our findings uncover that m^6A methylation regulates ripening of non-climacteric strawberry fruit by targeting ABA pathway, which is distinct from that in climacteric tomato fruit.

Key words

m^6A methylation, m^6A methyltransferase, abscisic acid, mRNA stability, translation efficiency, strawberry, fruit ripening

Introduction

As the most prevalent chemical modification in eukaryotic messenger RNAs (mRNAs), N^6-methyladenosine (m^6A) has been demonstrated to functionally modulate multiple biological processes through interfering mRNA metabolism [1-4]. In mammals, m^6A methylation has been unveiled to play critical roles in regulating various physiological and pathological processes, such as embryonic and post-embryonic development, cell circadian rhythms, and cancer stem cell proliferation [5-10]. The m^6A marks in mammals are dominantly installed by the methyltransferase complex composed of the stable catalytic core that is formed by methyltransferase-like 3 (METTL3) and METTL14 [11-13], the Wilms tumor 1-associating protein (WTAP) [14], and other concomitant functional elements [15-17]. The removal of m^6A marks is executed by two m^6A demethylases, fat mass and obesity-associated protein (FTO) and alkylated DNA repair protein AlkB homolog 5 (ALKBH5) [18, 19]. The m^6A modification are recognized by the reader proteins, such as YTH-domain family proteins and specific RNA binding proteins (RBPs), which mediate the downstream effects of m^6A methylation [4]. In plants, the m^6A methylation machineries have been characterized in the model plant *Arabidopsis thaliana* to modulate development processes such as shoot stem cell proliferation, trichome branching, and floral transition [20-23]. Moreover, m^6A has been demonstrated to play pivotal roles in mediating sporogenesis in rice [24] and regulating stress responses in maize [25]. By contrast, the m^6A methylation machineries as well as the characteristics and functions of m^6A in regulating physiological processes of horticultural crops remain largely unknown.

Fleshy fruits, which are enriched with nutrients, such as flavor compounds, fiber, vitamins

and antioxidants, represent one of the commercially valuable structures of horticultural crops. As an important component of diets, fleshy fruits are indispensable for human health [26]. The ripening of fleshy fruits, which is characterized by dramatic changes in color, texture, flavor and aroma compounds [27], is a complex, genetically programmed process that impacts fruit nutritional quality and shelf life. Fruit ripening is regulated by both environmental and internal cues, including light, temperature, phytohormones, and developmental genes [28, 29]. Based on the different ripening mechanisms, fruits are classified into two groups: climacteric (e.g. tomato, apple, banana, and avocado) and non-climacteric (e.g. strawberry, grape, and citrus) [30]. Phytohormone ethylene is essential for the ripening of climacteric fruits [31, 32], and substantial insights have been made toward ethylene biosynthesis, ethylene perception and signal transduction, and downstream gene regulation [33]. In comparison, the ripening of non-climacteric fruits is thought to be abscisic acid (ABA)-dependent [32, 34], although the regulation of ABA pathway is poorly understood. A comprehensive understanding of the common regulatory mechanisms underlying ripening in climacteric and non-climacteric species has great potential for improving fruit quality and maintaining shelf-life.

Recently, it was shown that epigenetic marks, including DNA methylation and histone posttranslational modifications, play critical roles in the regulation of fruit ripening [35]. In a previous study, we uncovered that mRNA m^6A methylation, which is considered as an mRNA "epitranscriptome", exhibits dynamic changes during fruit ripening of tomato, a typical climacteric fruit [36]. Mutation of *SlALKBH2*, the m^6A RNA demethylase gene, delays fruit ripening [36], indicating that m^6A modification participates in the ripening control of

87 climacteric fruit tomato. However, whether m^{6}A is evolutionarily conserved among different
88 types of fruits has not been defined. Moreover, the regulatory function of m^{6}A in ripening of
89 non-climacteric fruits remains elusive.

90 In the present study, we performed transcriptome-wide m^{6}A methylation (m^{6}A methylome)
91 in strawberry, a classical non-climacteric fruit, and revealed that m^{6}A represents a prevalent
92 modification in the mRNAs of strawberry fruit. Compared to the dynamic changes in m^{6}A
93 modification around the stop codons or within the 3' untranslated regions during the ripening
94 of tomato fruit, a specific enrichment of m^{6}A in the coding sequence (CDS) region, which
95 tends to be positively correlated with the abundance of the transcripts, was observed in the
96 ripe strawberry fruit. We demonstrated that, mediated by the methyltransferases MTA and
97 MTB, m^{6}A modification enhances mRNA stability or promotes translation efficiency of
98 genes in the ABA biosynthesis and signaling pathway, thereby facilitating the ripening of
99 strawberry fruit. Our study uncovers the regulatory effects of m^{6}A methylation on
100 non-climacteric strawberry fruit ripening, and reveals a direct role for m^{6}A methylation in the
101 regulation of key elements in the ABA pathway.

102

103 ## Results

104 ### m^{6}A methylation is a common feature of mRNAs in strawberry fruit

105 To investigate whether m^{6}A methylation participates in modulating ripening of
106 non-climacteric fruits, we performed m^{6}A-seq [37] to characterize m^{6}A methylomes on
107 diploid woodland strawberry (*Fragaria vesca*) at three developmental stages, i.e. S6 (the
108 growth stage 6, approximately 15 days post-anthesis (DPA)), RS1 (the ripening stage 1, 21

DPA), and RS3 (the ripening stage 3, 27 DPA) (Fig. 1a) [38]. The transition from S6 to RS1 represents the initiation of ripening, and that from RS1 to RS3 indicates the phase after ripening initiation. The m^6A methylome libraries were prepared with three independently biological replicates and subjected to massively parallel sequencing according to the standard m^6A-seq protocols [37]. High Pearson correlation coefficients were observed between biological replicates, indicating reliable repeatability (Additional file 1: Figure S1, S2). A total of 24-37 million raw reads were generated for each library (Additional file 2: Table S1), and this sequencing depth is comparative to that observed in mammal (11-24 million reads) [39], rice (23-47 million reads) [40], and tomato (20-30 million reads) [36]. After adaptor trimming and reads filtration, 24-37 million clean reads were remained at each library, and almost 95% of these reads were uniquely aligned to the strawberry genome v1.1, representing high mapping quality (Additional file 2: Table S1). The peak-calling algorithm was used to identify m^6A peaks with an estimated false discovery rate (FDR) < 0.05 [37], and only those consistently detected in all three biological replicates, which we called confident m^6A peaks, were used for subsequent analysis. We identified 9778, 10853 and 10095 confident m^6A peaks within 8934, 8990 and 8374 gene transcripts, in fruit at S6, RS1, and RS3, respectively (Fig. 1b; Additional file 2: Table S2-S4).

The m^6A-seq results were validated by independent m^6A immunoprecipitation followed by qPCR (m^6A-IP-qPCR) analysis. Three m^6A peak-containing transcripts, as well as three m^6A peak-free transcripts were randomly selected and examined (Additional file 1: Figure S3a). As expected, m^6A enrichment was only observed in transcripts containing m^6A peaks, but not in those without m^6A peaks (Additional file 1: Figure S3b), indicating that our m^6A-seq data

were accurate and robust.

Based on the parallel RNA-seq analyses, we estimated that the transcriptome of diploid woodland strawberry contains 0.6-0.7 m^6A peaks per actively expressed transcript, which shows FPKM (fragments per kilobase of transcript per million fragments mapped) ≥ 1 (Additional file 2: Table S5). These levels are comparable with those observed in *Arabidopsis* or tomato [36, 41], demonstrating that m^6A modification is a common feature of mRNA in strawberry fruit. Most of the m^6A-containing transcripts (>86%) possess one m^6A peak. Intriguingly, the percentage of transcripts harboring two or more m^6A peaks increases dramatically when the strawberry fruit turn to ripen, which changes from 2.95% at S6 to 13.07% at RS1, and 13.63% at RS3 (Fig. 1c), raising the possibility that new m^6A peaks generate at the initiation stage of ripening. Gene Ontology (GO) enrichment analysis indicated that m^6A modification appears in genes in multiple signaling pathways and cellular processes (Fig. 1d).

m^6A distribution exhibits a dramatic change at the initiation stage of strawberry fruit ripening

We then evaluated the distribution of m^6A peaks in the whole transcriptome of strawberry fruit. The transcript was divided into five non-overlapping segments: transcription start site (TSS, 100-nucleotide window centered on the TSS), 5' untranslated region (UTR), coding sequence (CDS), stop codon (100-nucleotide window centered on the stop codon), and 3' UTR. As shown in Fig. 2a, m^6A modifications in all three samples (fruit at S6, RS1, and RS3 stages) were highly enriched around the stop codon and within the 3' UTR, but the

153 percentage of peak summits within these regions declined markedly in the ripening process
154 (from S6 to RS1 or RS3; indicated by green arrowheads). Surprisingly, a substantial increase
155 in percentage of peak summits was concurrently observed in the CDS region adjacent to the
156 start codon in fruit at RS1 or RS3 compared to those at S6 (indicated by red arrowheads).
157 This is different from that observed in tomato, which shows no dramatic changes in
158 percentage of peak summits at the initiation stage of ripening [36].

159 The percentage of peak summits locating in the CDS region increased from 5.18% to 23.26%
160 from S6 to RS1, but displayed no distinct changes from RS1 to RS3 (Fig. 2b). In comparison,
161 the percentage of peak summits felling into the stop codon region and the 3' UTR decreased
162 from 39.95% and 53.81%, to 34.22% and 38.99%, respectively, from S6 to RS1, with no
163 obvious changes observed from RS1 to RS3 (Fig. 2b). After segment normalization by the
164 relative fraction that each segment occupied in the transcriptome, the m^6A enrichment in fruit
165 at RS1 or RS3 consistently exhibit a preferential localization in CDS region, besides enriched
166 around the stop codon and within the 3' UTR (Fig. 2c). Thus, the transcriptome-wide m^6A
167 distribution displays a dramatic change at the initiation stage of ripening, but not after
168 ripening initiation.

169 Several high-confidence sequence motifs were identified within the m^6A peaks (Additional
170 file 1: Figure S4), by using the hypergeometric optimization of motif enrichment (HOMER;
171 http://homer.ucsd.edu/homer/) [42]. The conserved RRACH consensus sequence observed in
172 mammals [43], where R represents adenosine (A) or guanosine (G), underlined A indicates
173 m^6A, and H represents A, cytidine (C), or uridine (U), appears in the list, whereas the UGUA
174 sequence motif found in *Arabidopsis* [22], tomato [36], and maize [25] was not identified.

These data suggest the complexity of m^{6}A modification among various species.

m^{6}A methylation overall affects mRNA abundance during the ripening of strawberry fruit

To gain insight into the potential roles of m^{6}A in the regulation of strawberry fruit ripening, we next sought for transcripts showing differential m^{6}A peaks, which exhibit a fold change ≥ 1.5 and *P* value < 0.05 in m^{6}A enrichment between the samples, by comparing the m^{6}A methylomes. A total of 1608 hypermethylated m^{6}A peaks and 865 hypomethylated m^{6}A peaks, corresponding to 1398 and 790 transcripts, respectively, were identified in fruit at RS1 compared to those at S6 (Fig. 3a; Additional file 2: Table S6, S7). By contrast, only 113 hypermethylated m^{6}A peaks and 102 hypomethylated m^{6}A peaks, which were distributed in 107 and 90 transcripts, respectively, were identified in fruit at RS3 compared to those at RS1 (Fig. 3b; Additional file 2: Table S8, S9). These results confirmed that substantial changes in overall m^{6}A methylome occurred at the initiation stage of ripening (from S6 to RS1), but not after ripening initiation (from RS1 to RS3).

The 1608 hypermethylated m^{6}A peaks were highly enriched (83.04%) in the CDS region, whereas the 865 hypomethylated m^{6}A peaks were mainly distributed around the stop codon (40.66%) or within the 3' UTR (58.59%) (Fig. 3c). This is in accordance with the results of m^{6}A distribution (Fig. 2), showing that the percentage of peak summits locating in the CDS region increased sharply, while that around the stop codon or within the 3' UTR declined, during from S6 to RS1. Interestingly, of the 1608 hypermethylated m^{6}A peaks, 1424 (88.56%) fell into the newly generated peaks, which represents ripening-specific peaks (Additional file

197 2: Table S10). For the differential m^{6}A peaks identified after ripening initiation, both the
198 hypermethylated and hypomethylated m^{6}A peaks were highly enriched (over 90%) around
199 the stop codon or within the 3' UTR (Fig. 3d).

200 Accumulating evidences have confirmed that m^{6}A deposition affects mRNA abundance [1,
201 22, 41, 44]. To assess the potential correlation between m^{6}A modification and mRNA
202 abundance in strawberry fruit, we compared the list of transcripts harboring altered m^{6}A
203 methylation with the differentially expressed genes (fold change $\geq$ 1.5 and *P* value < 0.05)
204 obtained from our parallel RNA-seq analyses (Additional file 2: Table S11, S12). Among the
205 1398 transcripts with hypermethylated m^{6}A peaks in fruit at RS1 compared to those at S6,
206 440 and 147 transcripts displayed higher and lower expression levels, respectively (Fig. 3e;
207 Additional file 2: Table S13). The distribution features of m^{6}A modifications in these
208 transcripts (Fig. 3c) suggest that m^{6}A depositions in CDS region overall exhibit a positive
209 effect on mRNA abundance. Accordingly, among the 790 transcripts showing
210 hypomethylated m^{6}A peaks in fruit at RS1 compared to those at S6, 267 transcripts showed
211 higher expression levels, whereas only 51 transcripts exhibited lower expression levels (Fig.
212 3f; Additional file 2: Table S14). The negative role of m^{6}A modifications on mRNA
213 abundance was also observed in transcripts with hypermethylated (Fig. 3g) or
214 hypomethylated (Fig. 3h) m^{6}A peaks that were identified after ripening initiation (Additional
215 file 2: Table S15, S16). Considering the distribution characteristics of m^{6}A within these
216 transcripts (Fig. 3c, d), it was proposed that, consistent with the observation in tomato fruit
217 [36], m^{6}A depositions around the stop codon or within the 3' UTR are generally negatively
218 correlated with the abundance of the transcripts in strawberry fruit.

To further evaluate the potential correlation between m^6A deposition and mRNA abundance, the changes in transcript levels were separately explored, based on the m^6A distributions, for transcripts showing differential m^6A modification at the initiation stage of ripening (from S6 to RS1). Gene expression profiles showed that most of the differential m^6A-modified transcripts (approximately 75%) of the 5' UTR, CDS, stop codon, and 3' UTR categories exhibited relatively higher transcript levels (Fig. 3i), suggesting that m^6A methylation overall affects mRNA abundance upon initiation of strawberry fruit ripening. Notably, 73 transcripts concurrently harboring hypermethylated m^6A peaks in the CDS region and hypomethylated m^6A peaks around the stop codon or within the 3' UTR were identified at this process. Of these, 34 transcripts were expressed at higher levels in fruit at RS1 compared to those at S6, while only 2 were expressed at lower levels (Fig. 3j), implying that the effects of m^6A methylation on the abundance of the transcripts may be overlaid.

Notably, hundreds of ripening-induced and ripening-repressed genes, which display significantly higher or lower expression in RS1 compared to S6 (Additional file 2: Table S11), exhibit differential m^6A modification (Additional file 2: Table S13, S14), implicating the involvement of m^6A methylation in the regulation of strawberry fruit ripening.

Genes in ABA biosynthesis and signaling pathway exhibit differential m^6a methylation upon ripening initiation

The plant hormone ABA has been elucidated to be essential for strawberry fruit ripening [32]. Two core ABA signal transduction pathways, the 'ABA-PYR/PYL-PP2C-SnRK2-AREB/ABF' pathway [45, 46] and the

241 'ABA-ABAR-WRKY40-ABI5' pathway [47], have been proposed in *Arabidopsis*,
242 respectively (Fig. 4a). In the m^{6}A-seq analysis, we found that transcripts of key genes in ABA
243 biosynthesis and signaling pathway, including *9-cis-epoxycarotenoid dioxygenase 5* (*NCED5*)
244 [38], *putative ABA receptor* (*ABAR*) [34], and *ABA-responsive element-binding protein 1*
245 (*AREB1*) [46], exhibit hypermethylation in the CDS region at the initiation stage of
246 strawberry fruit ripening (from S6 to RS1) (Fig. 4b, c). *NCED5* encodes the rate-limiting
247 enzyme for ABA biosynthesis, while *ABAR* and *AREB1* encode an ABA receptor and an
248 ABA-responsive element, respectively. All three genes have been proposed to regulate
249 strawberry fruit ripening [34, 38, 48]. The differential m^{6}A modifications were confirmed by
250 m^{6}A-IP-qPCR analysis (Fig. 4d). The transcript levels of *NCED5* and *AREB1*, but not *ABAR*,
251 increased significantly in fruit at RS1 compared to those at S6 as revealed by both RNA-seq
252 (Fig. 4e) and quantitative RT-PCR analyses (Fig. 4f), indicating a positive correlation
253 between m^{6}A depositions and mRNA abundances. It is noteworthy that similar results of m^{6}A
254 enrichment as well as transcript levels of these three genes were found upon ripening
255 initiation of the octoploid cultivated strawberry (*Fragaria* × *ananassa*) (Additional file 1:
256 Figure S5).

257 To better understand how m^{6}A methylation affects the abundance of the transcripts, we
258 examined the mRNA stability of *NCED5*, *AREB1*, and *ABAR* by monitoring the degradation
259 rate of mRNAs in the presence of transcription inhibitor actinomycin D. The intact CDS
260 sequences of the three genes and their mutated forms in which the potential m^{6}A sites
261 identified in m^{6}A-seq were mutated from A to cytidine (C) or guanosine (G) were separately
262 inserted into the vector for transient expression in the *Nicotiana benthamiana* leaves (Fig. 4g).

As shown in Fig. 4h, the mRNAs of *NCED5*, *AREB1*, and *ABAR* degraded obviously after actinomycin D treatment. The degradation rate was substantially increased for mRNAs of *NCED5* and *AREB1*, but not *ABAR*, in the mutated form (Fig. 4h), concomitant with significantly diminished m^6A depositions (Fig. 4i), indicating that site-specific m^6A modification stabilizes mRNAs of *NCED5* and *AREB1*.

The m^6A modification in the CDS region has been demonstrated to affect translation efficiency beyond mRNA stability [3]. We next investigated whether m^6A methylation modulates translation efficiency of *NCED5*, *AREB1*, and *ABAR*, which was determined by calculating the abundance ratio of mRNA in the polysomal RNA versus the total RNA [49] (Fig. 4j). The translation efficiency of *ABAR* rather than *NCED5* and *AREB1* was significantly decreased when the potential m^6A modification site was mutated (Fig. 4k), demonstrating that m^6A methylation facilitates translation of *ABAR*. Collectively, these data suggest that critical genes in ABA pathway undergo m^6A-mediated post-transcriptional regulation, which promotes mRNA stability or facilitates translation.

Characterizations of m^6A methyltransferases in strawberry fruit

Having observed the changes in m^6A methylation in a large number of transcripts (Fig. 3), including those of ABA biosynthesis and signaling genes (Fig. 4), during the ripening of strawberry fruit, we next explored the mechanistic basis. We speculate that the ripening-specific hypermethylation in the CDS region is regulated by mRNA m^6A methyltransferases. In mammals, METTL3 and METTL14 form a stable heterodimer wherein METTL3 serves as the m^6A catalytic subunit and METTL14 facilitates RNA binding [12, 13]

(Fig. 5a). The m^6A methyltransferase complexes are conserved between mammals and plants [50], and the *Arabidopsis* mRNA adenosine methyltransferase (MTA) and MTB appears to be the homologs of METTL3 and METTL14, respectively [51, 52]. We identified the single homologs of *Arabidopsis* MTA and MTB in the genome of the diploid woodland strawberry. Phylogenetic analysis indicated that MTA and MTB exhibit high similarity among plant species and are evolutionarily conserved with mammal METTL3 and METTL14 (Fig. 5b). Both MTA and MTB in strawberry contain the highly conserved MT-A70 domain (Additional file 1: Figure S6), which displays extremely similar protein sequences to those observed in mammals and *Arabidopsis* (Additional file 1: Figure S7).

Transcriptome analysis showed that *MTA* and *MTB* increased significantly at the initiation stage of ripening (from S6 to RS1) (Fig. 5c). The homolog genes of *MTA* and *MTB* in the octoploid cultivated strawberry also exhibited increased expression from white (Wt) stage to initial red (IR) stage (Fig. 5d, e), suggesting that the two methyltransferases may play important roles in modulating strawberry fruit ripening.

To explore the possibility that MTA and MTB in strawberry function in the form of heterodimer as METTL3 and METTL14 in mammals [12, 13], we subsequently analyzed the interactions between MTA and MTB using the yeast two-hybrid (Y2H) system. As shown in Fig. 5f, the yeast cells co-expressing AD-MTA and BD-MTB, but not the negative controls, displayed normal growth on the selective SD/-Leu-Trp-His (-LWH) and SD/-Leu-Trp-His-Ade (-LWHA) solid medium and turn to blue with the addition of X-α-gal, indicating that MTA interacts with MTB. The interactions between MTA and MTB were further verified by the split luciferase complementation imaging (LCI) assay, in which the

luciferase activity was detected when MTA-nLUC and cLUC-MTB were co-expressed in *N. benthamiana* leaves (Fig. 5g). It should be noted that, compared with the MT-A70 domain of MTB, the full-length MTB protein exhibit relatively weaker combining capacity with MTA (Fig. 5g). Subcellular localization analysis by transiently expressing MTA-mCherry and MTB-eGFP fusion proteins in *N. benthamiana* leaves showed that MTA is present in both the nucleus and cytoplasm, while the MTB protein is specifically localized in the nucleus (Fig. 5h). Interestingly, when MTA-mCherry was co-expressed with MTB-eGFP, the two proteins tend to colocalization in the nucleus (Fig. 5i).

m^{6}A methyltransferases positively regulate strawberry fruit ripening

We subsequently examined the function of MTA and MTB in strawberry fruit ripening. The RNA interference (RNAi) and overexpression constructs of *MTA* or *MTB* under the control of a 35S cauliflower mosaic virus promoter were agroinfiltrated into the octoploid strawberry fruit according to the reported procedures [53]. By comparing the fruits of RNAi with the control, we found that suppression of either *MTA* or *MTB* delayed fruit ripening (Fig. 6a). A visible color change was observed at the seventh days after agroinfiltration in the control, whereas the *MTA* or *MTB* RNAi fruits were almost green at this stage (Fig. 6a). Conversely, overexpression of *MTA* or *MTB* accelerated fruit ripening (Fig. 6a). Gene expression analysis indicated that *MTA* and *MTB* were successfully silenced in the RNAi fruits while enhanced in the overexpressed fruits (Fig. 6b). The ripening genes *chalcone synthase* (*CHS*) and *polygalacturonase 1* (*PG1*) displayed a noticeable decrease in the *MTA* or *MTB* RNAi fruits, but were dramatically enhanced in the overexpressed fruits (Fig. 6b). These results suggest

329 that *MTA* and *MTB* are necessary for normal fruit ripening of strawberry.

330 We next explored how the ripening of strawberry was regulated by MTA, the core
331 component of the methyltransferase complexes with m^6A catalytic activity. The
332 *MTA*-overexpressed fruits displayed higher m^6A levels than the control as revealed by
333 LC-MS/MS (Fig. 6c). RNA immunoprecipitation (RIP) analysis indicated that the MTA
334 directly binds to the transcripts of the ABA biosynthesis or signaling genes *NCED5*, *ABAR*,
335 and *AREB1* (Fig. 6d). Accordingly, the m^6A enrichments in the transcripts of *NCED5*, *ABAR*,
336 and *AREB1* (Fig. 6e) and the corresponding mRNA levels (Fig. 6f) were significantly
337 increased in the overexpressed fruits compared to the control. The mRNA stability assay
338 demonstrated that mRNA of *NCED5* and *AREB1*, but not that of *ABAR*, degraded more
339 slowly in the *MTA*-overexpressed fruits compared to the control (Fig. 6g). By contrast, *MTA*
340 overexpression markedly enhanced the translation efficiency of the *ABAR* mRNA, but
341 showed no significant effects on that of *NCED5* and *AREB1* (Fig. 6h). Together, these results
342 suggest that MTA may regulate strawberry fruit ripening by targeting genes in the ABA
343 pathway, leading to the increase in mRNA stability or translation efficiency of these genes.

344

345 **MTA-mediated m^6A methylation modulates genes encoding translation initiation factors**
346 **and elongation factors**

347 Due to the critical role of ABA in the regulation of fruit ripening of strawberry, we evaluated
348 whether *MTA* overexpression affects translation efficiency of other gene in the ABA signaling
349 pathway. We found that genes, such as *WRKY DNA-binding protein 40* (*WRKY40*), exhibited
350 significantly enhanced translation efficiency when the MTA was overexpressed (Additional

file 1: Figure S8). This could not be reasonably explained by m^{6}A deposition because the transcripts of these genes are not m^{6}A-modified according to our m^{6}A-seq datasets. We speculate that MTA may regulate translation efficiency of numerous transcripts beyond direct m^{6}A installation. As expected, *MTA* overexpression also elevated the translation efficiency of a number of transcripts of ripening-related genes without m^{6}A modification, such as *PG1* relevant to firmness and *dihydroflavonol 4-reductase* (*DFR*) associated with anthocyanin biosynthesis (Additional file 1: Figure S8).

To investigated the possible mechanisms, we mined our m^{6}A-seq and RNA-seq data and found that the transcripts of genes encoding translation initiation factors (*EIF2*, *EIF2B*, *EIF3A*, and *EIF3C*) and elongation factors (*EF1A*), which play pivotal roles in facilitating protein synthesis by promoting the initiation and elongation of mRNA translation, respectively, exhibited m^{6}A hypermethylation in the CDS region upon ripening initiation of strawberry fruit (Fig. 7a, b), concomitant with an increase in the transcript levels of these genes (Fig. 7c). Similar results were observed in the ripening process of the octoploid strawberry fruit (Fig. 7d, e). RIP analysis showed direct interactions between MTA and the transcripts of *EIF2*, *EIF2B*, *EIF3A*, and *EIF3C*, and *EF1A* (Fig. 7f). More importantly, the m^{6}A enrichment in these gene transcripts (Fig. 7g) and the mRNA abundance (Fig. 7h) increased noticeably when *MTA* was overexpressed. The mRNA degradation rates were obviously reduced in the *MTA*-overexpressed fruits compared to the control (Fig. 7i), implying that *MTA*-mediated m^{6}A modification stabilizes mRNAs of these genes. We propose that, in addition to direct modulation of translation efficiency via m^{6}A installation in the target transcripts, MTA may indirectly modulate translation efficiency via m^{6}A-mediated

regulation of the translation initiation factors or elongation factors.

Discussion

m^{6}A methylation participates in the regulation of strawberry fruit ripening

Compared to the understanding of the molecular basis underlying fruit ripening in climacteric fruits such as tomato, our knowledge regarding the regulation of ripening in non-climacteric fruits, e.g. strawberry, is still limited. Recently, it was elucidated that the ripening of strawberry involves the remodeling of DNA methylation [54]. However, it is unclear whether m^{6}A methylation, which has been revealed to modulate the ripening of tomato fruit [36], is involved in the regulation of strawberry fruit ripening. In the present study, we found that m^{6}A methylation represents a widespread mRNA modification in strawberry fruit and exhibits a dramatic change at the initiation stage of ripening. Overexpression of *MTA* or *MAB*, the m^{6}A methyltransferase genes, promotes fruit ripening, whereas repression of either gene delays ripening (Fig. 6a, b), demonstrating that m^{6}A methylation participates in the regulation of strawberry fruit ripening.

The transcript levels of *MTA* and *MTB* increased significantly upon ripening initiation of strawberry fruit (Fig. 5c-e), which may account for the m^{6}A hypermethylation in the CDS region. It should be noted that the m^{6}A methyltransferase genes in tomato express stably and no obviously global m^{6}A hypermethylation was observed during fruit ripening [36]. By contrast, it is the m^{6}A demethylase SlALKBH2 that positively regulates tomato fruit ripening through mediating the mRNA stability of *SlDML2*, a key DNA demethylase gene determining the DNA methylation patterns during ripening [36]. Due to the pivotal role of DNA

395 methylation in the regulation of fruit ripening in both climacteric and non-climacteric fruits, it
396 is reasonable to assume that m^6A modification may modulate strawberry fruit ripening by
397 modulating the DNA methylation machinery.

398 Strawberry undergoes an overall loss of DNA methylation during ripening, and the
399 reprogramming is governed by components in the RNA-directed DNA methylation (RdDM)
400 pathway rather than those in the demethylation pathway [54]. However, our m^6A-seq data
401 indicated that there was no differential m^6A modification in the transcripts of DNA
402 methyltransferase genes in the RdDM pathway during strawberry fruit ripening (Additional
403 file 1: Figure S9), suggesting that distinct mechanisms underlie the m^6A-mediated ripening
404 regulation in strawberry fruit.

405

406 **m^6A methylation regulates strawberry fruit ripening by targeting ABA pathway**

407 The phytohormone ABA plays crucial roles in plant growth, development, and stress
408 responses [55]. The ripening of non-climacteric fruits, such as strawberry, has been revealed
409 to be ABA-dependent [34]. Identification and functional definition of the core elements in
410 ABA biosynthesis and signal transduction pathway have expanded our understanding of the
411 mechanistic roles of ABA-mediated regulation of non-climacteric fruit ripening.

412 The ABA biosynthesis rate-limiting enzyme NCED was reported to play an essential role
413 in the ripening of strawberry fruit [34, 38]. Moreover, several critical constituents of ABA
414 signaling, including the ABA receptor FaPYR1 and FaABAR, the type 2C protein
415 phosphatase FaABI1, and the SNF1-related kinase FaSnRK2.6, have been revealed to be
416 indispensable for normal fruit ripening of strawberry [56-58]. Nevertheless, the regulatory

417 mechanisms underlying ABA biosynthesis and signaling pathway remain largely unknown.
418 In *Arabidopsis*, ABA receptor PYLs could be regulated by post-translational modification,
419 such as phosphorylation [59], tyrosine nitration [60], and ubiquitination [61], which
420 synergistically modulate the abundance and activity of the receptors [55]. In contrast, the
421 downstream signal molecules PP2Cs and SnRK2s are mainly controlled by protein
422 phosphorylation and dephosphorylation for maintaining the appropriate ABA signal
423 transduction [62-65]. The transcription of genes in ABA biosynthesis and signaling pathway
424 displays dynamic changes in various development processes or in response to environmental
425 stresses [55, 66-68], implying that they undergo precise regulation at transcriptional level.
426 However, little is known about the regulation of genes in ABA pathway at the
427 post-transcriptional level.

428 In this study, we found that *NCED5*, *ABAR*, and *AREB1*, the genes in ABA biosynthesis
429 and signaling pathway undergo m^6A-mediated post-transcriptional regulation (Fig. 4). The
430 m^6A modifications promote the mRNA stability of *NCED5* and *AREB1*, while enhance the
431 translation efficiency of *ABAR*. These findings identify a novel layer of gene regulation in
432 ABA biosynthesis and signaling pathway and establish a link between m^6A-mediated ABA
433 pathway and strawberry fruit ripening. Given the essential roles of ABA in plant development
434 and stress resistance, it is interesting and necessary to explore the regulation of m^6A
435 methylation on these physiological processes.

436

437 **m^6A modification exhibits diverse effects on mRNAs in strawberry**

438 As the most prominent modification in mRNA, m^6A was initially thought to accelerate

439 degradation of mRNAs through promoting their transfer from the translatable pool to the
440 decay sites [1]. Later findings have indicated that m^{6}A modification also harbors the capacity
441 to stabilize the mRNAs or promotes the translation in various biological processes [3, 22, 69,
442 70], although the underlying mechanisms are poorly understood, suggesting that m^{6}A
443 methylation possesses different regulatory roles on mRNAs [4]. This functional diversity was
444 proposed to be heavily dominated by m^{6}A distribution and the local sequence contexts within
445 transcripts. One likely explanation is that the specific sequence contexts around m^{6}A marks
446 determine the recruitment of diverse m^{6}A readers or other RNA binding proteins (RBPs) that
447 carry distinguishing and even opposite molecular functions [4].

448 In this study, we observed a dramatic change in m^{6}A modification at the initiation of
449 strawberry fruit ripening (Fig. 2). The m^{6}A depositions in the CDS region tend to stabilize the
450 mRNAs, whereas those in the 3' UTR or around the stop codon exhibit the opposite effects
451 (Fig. 3). These data suggest that, depending on their distribution, the m^{6}A modification plays
452 distinct roles on mRNAs in strawberry. Notably, the differential m^{6}A modification in the
453 ripening process of tomato fruit mainly appeared around the stop codon or within the 3' UTR,
454 and these m^{6}A depositions were generally negatively correlated with the abundance of the
455 mRNAs. Combining the observation in strawberry and tomato, we propose that m^{6}A
456 modification around the stop codon or within the 3' UTR tends to negatively correlated with
457 mRNA abundance in the ripening process of both climacteric and non-climacteric fruits,
458 whereas m^{6}A deposition in the CDS region generally stabilize the mRNAs upon ripening
459 initiation of non-climacteric fruits. Interestingly, besides modulating mRNA stability, m^{6}A
460 modification also affected translation efficiency of some transcripts. The changes in

translation efficiency might be directly regulated by m^6A deposition on the transcripts, or indirectly by m^6A-mediated regulation of translation initiation factors and elongation factors.

In conclusion, our work reveals a regulatory role of m^6A methylation on the ripening of the non-climacteric strawberry fruit. The molecular basis, which involves the m^6A-mediated regulation of genes in the ABA biosynthesis and signaling pathway, is distinct from what was described in climacteric tomato fruit (Additional file 1: Figure S10). These findings provide new insights into understanding the regulatory networks controlling fruit ripening.

Methods

Plant materials

The diploid woodland strawberry (*Fragaria vesca* cv. 'Hawaii-4') and the octoploid cultivated strawberry (*Fragaria* × *ananassa* cv. 'Benihoppe') were planted in a greenhouse with standard culture conditions [58]. To accurately determine fruit ages through development, flowers were tagged at the anthesis. Fruits of 'Hawaii-4' at the growth stage 6 (S6), the ripening stage 1 (RS1), and the ripening stage 3 (RS3) [38], which were on average 15, 21, and 27 days post-anthesis (DPA), respectively, were harvested, and then frozen in liquid nitrogen. The fruits with the removal of attached achenes were subsequently stored at −80 °C until use. The 'Benihoppe' fruits were harvested at the small green (SG), large green (LG), white (Wt), initial red (IR), and full red (FR) stages, respectively, based on the size, weight, shape, and color [71], and then maintained at fresh status for further studies or directly frozen and stored as the 'Hawaii-4'.

m^6A-seq and data analysis

The m^6A-seq was performed according to the method described by Dominissini et al (2013) [37]. Briefly, total RNAs were extracted from the woodland strawberry fruit at S6, RS1, and RS3 stages by the plant RNA extraction kit (Magen, R4165-02), and then 300 μg of intact total RNAs were used for mRNA isolation by the Dynabeads mRNA purification kit (Life Technologies, 61006). The purified mRNAs were randomly fragmented into ~100 nucleotide-long fragments by incubation at 94 °C for 5 min in the RNA fragmentation buffer (10 mM Tris-HCl, pH 7.0, and 10 mM $ZnCl_2$). The reaction was terminated with 50 mM EDTA, and then the fragmented mRNAs were purified by standard phenol-chloroform extraction and ethanol precipitation. For immunoprecipitation (IP), 5 μg of fragmented mRNAs was mixed with 10 μg of anti-m^6A polyclonal antibody (Synaptic Systems, 202003) and incubated at 4 °C for 2 h in 450 μL of IP buffer consisting of 10 mM Tris-HCl, pH 7.4, 150 mM NaCl, 0.1% NP-40 (v/v), and 300 U mL^{-1} RNase inhibitor (Promega, N2112S). After the addition of 50 μL Dynabeads protein-A (Life Technologies, 10002A), the mixture was incubated at 4 °C for another 2 h. The beads were subsequently washed twice with high-salt buffer containing 50 mM Tris-HCl, pH 7.4, 1 M NaCl, 1 mM EDTA, 1% NP-40 (v/v), and 0.1% SDS (w/v) and twice with IP buffer. The m^6A-containing fragments were eluted from the beads by incubation with 6.7 mM N^6-methyladenosine (TargetMol, T6599) in IP buffer at 4 °C for 2 h, followed by standard phenol-chloroform extraction and ethanol precipitation. Then, 50 ng of m^6A-containing mRNAs or pre-immunoprecipitated mRNAs (the input) were used for library construction by the NEBNext ultra RNA library preparation kit (NEB, E7530). High-throughput sequencing was conducted on the illumina HiSeq X

505 sequencer with a paired-end read length of 150 bp following the standard protocols. The
506 sequencing was performed with three independent biological replicates, and each RNA
507 sample was prepared from the mix of at least 60 strawberry fruits to avoid individual
508 difference among fruits.

509 For data analysis, the quality of raw sequencing reads was initially assessed by FastQC
510 tool (version 0.11.7; http://www.bioinformatics.babraham.ac.uk/projects/fastqc). Adaptors
511 and low-quality bases with a score < 20 were trimmed using Cutadapt (version 1.16) [72],
512 and then short reads with a length < 18 nucleotides or reads containing ambiguous
513 nucleotides were filtered out by Trimmomatic (version 0.30) [73]. The remaining reads were
514 aligned to the strawberry reference genome v1.1
515 (ftp://ftp.bioinfo.wsu.edu/species/Fragaria_vesca/Fvesca-genome.v1.1) by Burrows Wheeler
516 Aligner (BWA; version 0.30) [74]. Mapping quality (MAPQ) of all aligned reads was
517 concurrently evaluated, and only uniquely mapped reads with a MAPQ ≥ 13 were retained
518 for subsequent analysis [37].

519 The identification of m^6A peaks was carried out by MACS software (version 2.0.10) [75],
520 using the corresponding input as a control. High-confidence peaks were obtained by a
521 stringent cutoff threshold for MACS-assigned false discovery rate (FDR) < 0.05.
522 PeakAnalyzer (version 2.0) [76] was applied to annotate the identified peaks to the
523 strawberry genome annotation file
524 (ftp.bioinfo.wsu.edu/species/Fragaria_vesca/Fvesca-genome.v2.0.a2/genes/). To identify the
525 differentially methylated peaks between samples, the m^6A site differential algorithm [77] was
526 applied with a criterion of fold change in m^6A enrichment ≥ 1.5 and *P* value < 0.05. HOMER

(version 4.7; http://homer.ucsd.edu/homer/) [78] was employed to identify the m^6A motifs with a restricted length of six nucleotides. The differential m^6A peaks identified between S6 and RS1 stages were used as the target sequences, and the exon sequences without m^6A peaks were used as the background sequences. Integrated Genome Browser (IGB, version 9.0.2) [79] was used for visualization of m^6A peaks. Gene Ontology (GO) enrichment was analyzed on the agriGO database (version 2.0; http://systemsbiology.cau.edu.cn/agriGOv2/) and only statistically significant terms with a Yekutieli-corrected *P* value < 0.05 were remained [80].

RNA-seq and data analysis

The sequencing reads from the input samples in m^6A-seq were used for RNA-seq analysis as previously reported [21]. In brief, the uniquely mapped reads with a MAPQ ≥ 13 were assembled by Cufflinks [81]. Gene expression was presented as fragments per kilobase of exon per million mapped fragments (FPKM) by using Cuffdiff [81], which concurrently provides statistical routines for capturing differentially expressed genes. The Benjamini and Hochberg's approach [82] was used to adjust the resulting *P* values for controlling the false discovery rate (FDR). Differential gene expression was defined on basis of a cutoff criterion of FPKM fold change ≥ 1.5 and *P* value < 0.05.

Quantitative RT-PCR analysis

Total RNAs were extracted from the strawberry fruits or *N. benthamiana* leaves using the plant RNA extraction kit (Magen, R4165-02). The extracted RNAs were reverse transcribed into cDNAs by the HiScript® III RT SuperMix for qPCR kit (Vazyme, R323-01). The

549 synthesized cDNAs were then employed as templates for PCR amplification using the
550 ChemQ Universal SYBR qPCR Master Mix (Vazyme, Q711-02-AA) and a StepOne Plus
551 Real-Time PCR System (Applied Biosystems) in the following program: 95 °C for 10 min,
552 followed by 40 cycles of 95 °C for 15 s and 60 °C for 30 s. Relative quantification of gene
553 transcription levels were performed by the cycle threshold (C_T) $2^{(-\Delta CT)}$ method [83].
554 Strawberry *ACTIN* (gene22626) or *N. benthamiana ACTIN* (*Niben101Scf03410g03002*) was
555 applied to normalize the expression values. The primers for PCR amplification are listed in
556 Additional file 2: Table S17. The experiment was conducted with three biological replicates,
557 and each contained three technical repeats.
558
559 **m^{6}A-IP-qPCR**
560 m^{6}A-IP-qPCR was carried out as previously described with minor modifications [84]. Briefly,
561 5 μg of intact mRNAs were fragmented into ~300 nucleotide-long fragments by an
562 incubation at 94 °C for 30 s in the RNA fragmentation buffer (10 mM Tris-HCl, pH 7.0, and
563 10 mM $ZnCl_2$), followed by the addition of 50 mM EDTA to terminate the reaction. The
564 fragmented mRNAs were purified by standard ethanol precipitation and resuspended in 250
565 μL of DEPC-treated water. Then, 5 μL of fragmented mRNAs was taken as the input control
566 and 100 μL were incubated with 5 μg of anti-m^{6}A polyclonal antibody (Synaptic Systems,
567 202003) at 4 °C for 2 h in 450 μL of IP buffer containing 10 mM Tris-HCl, pH 7.4, 150 mM
568 NaCl, 0.1% NP-40 (v/v), and 300 U mL^{-1} RNase inhibitor (Promega, N2112S). The mixture
569 was subsequently incubated with 20 μL of Dynabeads protein-A (Life Technologies, 10002A)
570 at 4 °C for another 2 h. After washing twice with high-salt buffer containing 50 mM Tris-HCl,

pH 7.4, 1 M NaCl, 1 mM EDTA, 1% NP-40 (v/v), and 0.1% SDS (w/v) and twice with IP buffer, the m^6A-containing fragments were eluted by an incubation with 6.7 mM N^6-methyladenosine (m^6A; TargetMol, T6599) in 200 μL of IP buffer at 4 °C for 2 h, followed by ethanol precipitation. The immunoprecipitated mRNA fragments were finally resuspended in 5 μL DEPC-treated water. Then, both the m^6A-containing mRNAs and the input mRNAs were submitted to quantitative RT-PCR by using the primers listed in Additional file 2: Table S17. Relative m^6A enrichment in specific region of a transcript was calculated using the cycle threshold (C_T) $2^{(-\Delta CT)}$ method [83]. The value for the immunoprecipitated sample was normalized against that for the input. The experiment was performed with three biological replicates, and each contained three technical repeats.

Identification of strawberry m^6A methyltransferases and phylogenetic analysis

To identify m^6A methyltransferases in strawberry, the amino acid sequence of conserved MT-A70 domain (PF05063) was downloaded from the Pfam (http://pfam.xfam.org/) and then utilized to search the potential homologs against the strawberry protein dataset (ftp.bioinfo.wsu.edu/species/Fragaria_vesca/Fvesca-genome.v2.0.a2/genes/) using HMMER 3.1 with default parameters [85]. The resulting protein sequences were analyzed on the CDD database (https://www.ncbi.nlm.nih.gov/cdd/) [86], and only that containing a MT-A70 domain were remained as the m^6A methyltransferase candidates. The known m^6A methyltransferases METTL3 and METTL14 in mammals and MTA and MTB in *Arabidopsis* were then employed to perform BLASTP-algorithm in NCBI (https://www.ncbi.nlm.nih.gov/) to further confirm the identified homologs. For phylogenetic analysis, the sequences of the

identified strawberry m^6A methyltransferase were aligned with the sequences of m^6A methyltransferase in mouse (*Mus musculus*), rice (*Oryza sativa*), maize (*Zea mays*), tomato (*Solanum lycopersicum*), tobacco (*Nicotiana benthamiana*), and *Arabidopsis*, using ClustalX 2.1 with standard parameters [87]. The alignment result was imported into MEGA software (version 5.2) to create the phylogenetic tree by using Neighbor-Joining method with 1000 bootstrap replicates [88].

Y2H analysis

Y2H analysis was performed as the previously described [89]. In brief, the coding sequence of *MTA* and *MTB* was amplified from the cDNAs of diploid woodland strawberry and then ligated into the pGADT7 (AD) and pGBKT7 (BD) vectors, respectively. The resulting plasmids were co-transformed into *Saccharomyces cerevisiae* strain AH109 according to the protocols in the Matchmaker GAL4 Two-Hybrid System 3 (Clontech). The yeast cells were cultured on SD/-Leu-Trp (-LW) medium, and then transferred onto the SD/-Leu-Trp-His (-LWH) or SD/-Leu-Trp-His-Ade medium (-LWHA) with or without X-α-gal. Transformants carrying empty pGADT7 (AD) or pGBKT7 (BD) vectors were used as negative controls, and that concurrently carrying pGBKT7-53 and pGADT7-T vectors was used as the positive control. The primers used for vector constructions are listed in Additional file 2: Table S17.

LCI assay

LCI assay was performed as previously reported [90]. Briefly, the coding sequence of *MTA* was cloned into the pCambia1300-nLUC plasmid, and the coding sequence of *MTB* or its

615 MT-A70 domain sequence (*MTB*^{D}) was cloned into the pCambia1300-cLUC plasmid. The
616 resulting constructs were separately transformed into *Agrobacterium tumefaciens* strain
617 GV3101. The agrobacteria were cultured at 28 °C for 18 h in Luria-Bertani (LB) liquid
618 medium containing 50 μg mL^{-1} kanamycin, 50 μg mL^{-1} gentamycin, and 50 μg mL^{-1}
619 rifampicin. After being pelleted by centrifugation at 5,000 g for 5 min, the agrobacteria were
620 resuspended in the infiltration buffer (10 mM MES, pH 5.6, 10 mM $MgCl_2$, and 100 μM
621 acetosyringone) to a final OD_{600} of 0.5. Then, the suspension was infiltrated into *N.*
622 *benthamiana* leaves for co-expression of fusion protein nLUC-MTA with MTB-cLUC or
623 MTB^{D}-cLUC. After culture for 36 h, the leaves were incubated with 1 mM luciferin dissolved
624 in ddH_2O supplemented with 0.01% Triton X-100 at room temperature for 5min, and then
625 observed under a chemiluminescence imaging system (Tanon). Empty vectors expressing
626 cLUC or nLUC were co-transformed as the negative controls. The primers used for vector
627 constructions are listed in Additional file 2: Table S17.
628
629 **Subcellular localization**
630 For subcellular localization analysis, the coding sequence of *MTA* and *MTB* was amplified
631 from the cDNAs of diploid woodland strawberry and then inserted into the
632 pCambia2300-mCherry and pCambia2300-eGFP plasmids to generate 35S::*MTA-mCherry*
633 and 35S::*MTB-eGFP* vectors, respectively. The resulting constructs were separately
634 transformed into *A. tumefaciens* strain GV3101. The agrobacteria were subsequently
635 infiltrated into *N. benthamiana* leaves for the individual expression of mCherry-tagged MTA
636 (MTA-mCherry) and eGFP-tagged MTB (MTB-eGFP) or the co-expression of the two fusion

637 proteins. After culture for 36 h, the mesophyll protoplasts were isolated from *N. benthamiana*
638 leaves as previously reported [91] and observed under a Leica confocal microscope (Leica
639 DMI600CS). Protoplasts expressing eGFP or mCherry were used as negative controls. The
640 primers used for vector constructions are listed in Additional file 2: Table S17.
641
642 **Agroinfiltration-mediated transient transformation in strawberry fruit**
643 Transient transformation of strawberry fruit mediated by agroinfiltration was performed as
644 previously described [53]. To construct the RNA interference (RNAi) vectors, a ~300 bp
645 fragment targeting the coding sequence region of *MTA* or *MTB* was cloned and inserted into
646 the pCR8 plasmid, and then restructured into the pK7GWIWGD (II) plasmid by using the
647 Gateway LR Clonase^{TM} Enzyme Mix (Invitrogen, 11791-020). To construct the
648 overexpression (OE) vectors, the coding sequence of *MTA* and *MTB* was amplified and
649 ligated into the pCambia2300-eGFP plasmid to generate 35S::*MTA-eGFP* and
650 35S::*MTB-eGFP* vector, respectively. The resulting constructs were separately transformed
651 into the *A. tumefaciens* strain GV3101. The agrobacteria were cultured at 28 °C overnight in
652 LB liquid medium supplemented with 50 μg mL^{-1} kanamycin, 50 μg mL^{-1} gentamycin, and
653 50 μg mL^{-1} rifampicin, and then diluted 1:100 in 100 mL of fresh LB medium to continue
654 culturing for approximately 8 h. The agrobacteria cells were subsequently collected by
655 centrifugation at 5,000 g for 5 min and resuspended in the infiltration buffer (10 mM MES,
656 pH 5.6, 10 mM $MgCl_2$, and 100 μM acetosyringone) to a final OD_{600} of 0.8. After being kept
657 at room temperature for 2 h without shaking, the suspensions were injected into the octoploid
658 strawberry fruit at large green (LG) stage by using a 1 mL syringe. The infiltrated fruits were

659 cultured for 5-7 days in a growth room with the following conditions: 23 °C, 80 % relative
660 humidity, and a 16/8 h light/dark photoperiod with a light intensity of 100 μmol m^{-2} s^{-1}. The
661 experiment was performed with three independent biological replicates, and each group
662 contained at least fifteen fruits. The primers used for vector constructions are listed in
663 Additional file 2: Table S17.
664
665 **mRNA stability assay**
666 For mRNA stability assay in *N. benthamiana* leaves, the coding sequence of *NCED5*, *ABAR*,
667 and *AREB1* was amplified from the cDNAs of diploid woodland strawberry. The mutated
668 forms of the amplified sequence in which the potential m^6A sites were replaced by cytidine
669 (C) or guanine (G) were constructed using the QuikChange II XL Site-directed Mutagenesis
670 Kit (Agilent Technologies, 200518). The fragments were separately inserted into the
671 pCambia2300 vector, which were subsequently transformed into *A. tumefaciens* strain
672 GV3101. Then, the agrobacteria were cultured at 28 °C for 18 h in LB liquid medium
673 containing 50 μg mL^{-1} kanamycin, 50 μg mL^{-1} gentamycin, and 50 μg mL^{-1} rifampicin. After
674 being collected by centrifugation at 5,000 g for 5 min, the agrobacteria were diluted to an
675 OD_{600} of 0.5 in the infiltration buffer (10 mM MES, pH 5.6, 10 mM $MgCl_2$, 100 μM
676 acetosyringone), and then infiltrated into the *N. benthamiana* leaves. After 36 h of incubation,
677 the infiltration parts in the leaves were injected with 20 μg mL^{-1} actinomycin D (Sigma,
678 A4262) dissolved in ddH_2O. After culture for 30 min, leaf discs were taken and considered as
679 time 0 controls, and subsequent samples were harvested every 3 h in triplicate.
680 For mRNA stability assay in strawberry, the *MTA*-overexpressed fruit and the control were

681 sliced into ~3 mm slices, and then transferred onto plates containing 20 μg mL^{-1} actinomycin
682 D dissolved in ddH_2O. After incubation for 30 min, the slices were collected as the *N.*
683 *benthamiana* leaf discs. The mRNA levels of genes were subsequently examined by
684 quantitative RT-PCR as described above. All primers used for PCR amplification were listed
685 in Additional file 2: Table S17.
686
687 **Translation efficiency assay**
688 Translation efficiency was assayed according to the method described by Merchante et al
689 (2015) [49]. Briefly, 6 g of strawberry fruits or 3 g of *N. benthamiana* leaves were ground
690 into fine powder in liquid nitrogen. One gram of sample was used for total RNA extraction,
691 and the rest was suspended in 15 mL of polysome extraction buffer (200 mM Tris-HCl, pH
692 9.0, 35 mM $MgCl_2$, 200 mM KCl, 25 mM EGTA, 1% Triton X-100 (v/v), 1% IGEPAL
693 CA-630 (v/v), 5 mM DTT, 1 mM PMSF, 50 μg mL^{-1} Chloramphenicol, and 100 μg mL^{-1}
694 Cycloheximide) at 4 °C for 20 min with slight shaking. The mixture was centrifuged twice at
695 16, 000 g for 20 min at 4 °C. Then, 12.5 mL of supernatant were slowly transferred onto 13.5
696 mL of sucrose buffer (1.75 M Sucrose, 400 mM Tris-HCl, pH 9.0, 35 mM $MgCl_2$, 5 mM
697 EGTA, 200 mM KCl, 5 mM DTT, 50 μg mL^{-1} Chloramphenicol, and 50 μg ml^{-1}
698 Cycloheximide). After centrifugation at 200,000 g for 4 h at 4 °C, the supernatant was
699 carefully removed, and the polysomes in the bottom were resuspended in 300 μL of
700 DEPC-treated water. The polysomal RNAs, as well as the total RNAs, were isolated by using
701 the plant RNA extraction kit (Magen, R4165-02), and used for quantitative RT-PCR analysis
702 as described above. Translation efficiency was calculated by the abundance ratio of mRNA in

the polysomal RNA versus the total RNA using the cycle threshold (CT) $2^{(-\Delta CT)}$ method [83] with the *GADPH2* gene as an internal reference. The primers used for PCR amplification are listed in Additional file 2: Table S17.

Quantitative analysis of m^6A level by LC-MS/MS

The global m^6A levels in strawberry fruit were detected by LC-MS/MS as previously described [36] with minor modifications. In brief, 200 ng of mRNAs was digested at 37 °C for 6 h with 1 unit of Nuclease P1 (Wako, 145-08221) in 50 μL of reaction buffer containing 10 mM ammonium acetate, pH 5.3, 25 mM NaCl, and 2.5 mM $ZnCl_2$. Then, 1 unit of alkaline phosphatase (Sigma-Aldrich, P6774) and 5.5 μL of 1 M fresh NH_4HCO_3 were added, followed by incubation at 37 °C for another 6 h. After centrifugation at 15,000 g for 5 min, the supernatant was used for LC-MS/MS analysis. The digested nucleosides were separated by UPLC (Waters, ACQUITY) equipped with a ACQUITY UPLC HSS T3 column (Waters), and then detected by a Triple Quad Xevo TQ-S (Waters) mass spectrometer in positive ion mode with multiple reaction monitoring. The mobile phase was composed of buffer A (0.1% formic acid in ultrapure water) and buffer B (100% acetonitrile). Nucleosides were accurately quantified depending on the nucleoside-to-base ion mass transitions of m/z 268.0 to 136.0 (A) and m/z 282.0 to 150.1 (m^6A). The pure commercial adenosine (A; TargetMol, T0853) and N^6-methyladenosine (m^6A; TargetMol, T6599) were used to generate standard curves, which were subsequently employed to calculate the contents of A and m^6A in each sample. The global m^6A levels were presented in the form of m^6A/A ratio. The experiment was repeated with three independent biological replicates.

725

726 **RNA immunoprecipitation**

727 RNA immunoprecipitation (RIP) was carried out following the method of Wei et al (2018)
728 [22] with minor modifications. Briefly, the octoploid strawberry fruit expressing the
729 MTA-eGFP protein were sliced into ~2 mm slices, and then fixed with 1% formaldehyde
730 under a vacuum for 30 min on ice. The fixation was terminated by the addition of 150 mM
731 glycine, followed by incubation on ice for 5 min. The fixed fruit tissues (2 g) were
732 homogenized in 5 mL of lysis buffer (50 mM HEPES, pH 7.5, 2 mM EDTA, 150 mM KCl,
733 0.5% NP-40 (v/v), 2 mM EDTA, 0.5 mM DTT, 1× cocktail protease inhibitor (Sigma,
734 04693132001), and 300 U mL^{-1} RNase Inhibitor). After incubation at 4 °C for 1 h, the
735 mixture was centrifuged at 15,000 g for 30 min. Then, 200 μL of the supernatant were taken
736 as the input control, and the remainder was subjected to immunoprecipitation (IP) with
737 anti-GFP monoclonal antibody or rabbit lgG at 4 °C overnight. Fifty microliters of
738 Dynabeads Protein-A (Life Technologies, 10002A) were added to the mixture and incubated
739 at 4 °C for 2 h. After washing four times with PBS buffer, the RNA-protein mix was
740 catalyzed by proteinase K (Takara, 9034) at 55 °C for 1 h. The immunoprecipitated mRNAs
741 and input mRNAs were subsequently isolated by the plant RNA extraction kit (Magen,
742 R4165-02). Relative enrichment of individual transcript was determined by quantitative
743 RT-PCR analysis as described above. The primers used for PCR amplification are listed in
744 Additional file 2: Table S17. The analysis was performed with three biological replicates, and
745 each contained three technical repeats.

746

Data access

The raw sequencing data and processed peaks data in m^6A-seq have been deposited in the Gene Expression Omnibus database under the accession number GSE167183. All the other data generated in this study are included in the article and the Additional files.

Additional material

Additional file 1: Supplementary Figure S1-S10. **Figure S1.** Pearson correlation analysis of input reads in the m^{6}A peak regions identified from m^{6}A-seq. **Figure S2.** Pearson correlation analysis of immunoprecipitation (IP) reads in the m^{6}A peak regions identified from m^{6}A-seq. **Figure S3.** Validation of confident m^{6}A peaks. **Figure S4.** Sequence motif identified within the m^{6}A peaks by HOMER (http://homer.ucsd.edu/homer/). **Figure S5.** m^{6}A modification and expression of genes in ABA biosynthesis and signaling pathway in octoploid cultivated strawberry. **Figure S6.** Identification of the conserved MT-A70 domain of m^{6}A methyltransferases MTA and MTB in diploid woodland strawberry and octoploid cultivated strawberry. **Figure S7.** Protein sequence alignment of the MT-A70 domains in m^{6}A methyltransferases. **Figure S8.** The changes in translation efficiency of ABA signaling gene and ripening genes in the MTA-overexpressed fruits. **Figure S9.** m^{6}A enrichment for DNA methyltransferase genes from m^{6}A-seq data. **Figure S10.** Regulatory model for the m6A-mediated ripening in climacteric tomato fruit and non-climacteric strawberry fruit.

Additional file 2: Supplementary Table S1-S17. **Table S1.** A summary of m^{6}A-seq information in strawberry fruit at different stages. **Table S2.** Confident m^{6}A peaks identified by three independent m^{6}A-seq experiments in strawberry fruit at S6 stage. **Table S3.** Confident m^{6}A peaks identified by three independent m^{6}A-seq experiments in strawberry fruit at RS1 stage. **Table S4.** Confident m^{6}A peaks identified by three independent m^{6}A-seq experiments in strawberry fruit at RS3 stage. **Table S5.** m^{6}A density in actively expressed transcripts. **Table S6.** Transcripts containing hypermethylated m^{6}A peak in strawberry fruit at

774 RS1 stage compared to those at S6 stage. **Table S7.** Transcripts containing hypomethylated
775 m^6A peak in strawberry fruit at RS1 stage compared to those at S6 stage. **Table S8.**
776 Transcripts containing hypermethylated m^6A peak in strawberry fruit at RS3 stage compared
777 to those at RS1 fruit. **Table S9.** Transcripts containing hypomethylated m^6A peak in
778 strawberry fruit at RS3 stage compared to those at RS1 stage. **Table S10.** Ripening-specific
779 peaks identified in strawberry fruit at RS1 stage. **Table S11.** Differentially expressed genes
780 between strawberry fruit at S6 and RS1 stage identified by three independent RNA-seq
781 experiments. **Table S12.** Differentially expressed genes between strawberry fruit at RS1 and
782 RS3 stage identified by three independent RNA-seq experiments. **Table S13.** Differentially
783 expressed genes containing hypermethylated m^6A peaks in strawberry fruit at RS1 stage
784 compared to those at S6 stage. **Table S14.** Differentially expressed genes containing
785 hypomethylated m^6A peaks in strawberry fruit at RS1 stage compared to those at S6 stage.
786 **Table S15.** Differentially expressed genes containing hypermethylated m^6A peaks in
787 strawberry fruit at RS3 stage compared to those at RS1 stage. **Table S16.** Differentially
788 expressed genes containing hypomethylated m^6A peaks in strawberry fruit at RS3 stage
789 compared to those at RS1 stage. **Table S17.** A summary of primer informations.

790

791 ## Abbreviations

792 ABA: abscisic acid; *ABAR*: *putative ABA receptor*; AD: activation domain; ALKBH: AlkB
793 homolog; *AREB1*: *ABA-responsive element-binding protein 1*; BD: binding domain; CDS:
794 coding sequence; *CHS*: *chalcone synthase*; *DFR*: *dihydroflavonol 4-reductase*; DPA: days
795 post-anthesis; EF: translation elongation factor; eGFP: enhanced green fluorescent protein;

796 EIF: translation initiation factor; FDR: false discovery rate; FPKM: fragments per kilobase of
797 transcript per million fragments mapped; FR: full red; FTO: fat mass and obesity-associated
798 protein; GO: gene ontology; HOMER: hypergeometric optimization of motif enrichment;
799 IGB: Integrated Genome Browser; IP: immunoprecipitation; IR: initial red; LB: Luria-Bertani;
800 LCI: luciferase complementation imaging; LG: large green; m^6A: N^6-methyladenosine;
801 MAPQ: mapping quality; METTL: methyltransferase like; mRNA: messenger RNA; MTA:
802 adenosine methyltransferase; MTB: adenosine methyltransferase B; *NCED5*:
803 *9-cis-epoxycarotenoid dioxygenase 5*; OE: overexpression; *PG1*: *polygalacturonase 1*; RBP:
804 RNA binding proteins; RdDM: RNA-directed DNA methylation; RIP: RNA
805 immunoprecipitation; RNAi: RNA interference; RS1: the ripening stage 1; RS3: the ripening
806 stage 3; RT-PCR: reverse transcription polymerase chain reaction; S6 :the growth stage 6; SG:
807 small green; TSS: transcription start site; UTR: untranslated region; *WRKY40*: *WRKY*
808 *DNA-binding protein 40*; Wt: white; WT: wild-type; WTAP: Wilms' tumor 1-associating
809 protein; Y2H: yeast two-hybrid.
810

811 ## Acknowledgements

812 We thank Hang Su (Institute of Botany, Chinese Academy of Sciences) for the assistance with
813 LC-MS/MS assay. We thank Jingquan Li (Institute of Botany, Chinese Academy of Sciences)
814 for the assistance with confocal microscopy assay. We also thank Jianmin Zhou (Institute of
815 Genetics and Developmental Biology, Chinese Academy of Sciences) for providing the
816 pCambia1300–nLUC/cLUC vectors.
817

Funding

This work was supported by the National Key Research and Development Program (2018YFD1000200) and the National Natural Science Foundation of China (grant Nos. 31925035, 31930086, and 31572174).

Availability of data and materials

The raw sequencing data and processed peaks data in m^6A-seq have been deposited in the Gene Expression Omnibus database under the accession number GSE167183 (https://www.ncbi.nlm.nih.gov/geo/query/acc.cgi?acc=GSE167183) with a temporary token of 'yjatoqksvribzkf'. All the other data generated in this study are included in the article and the Additional files.

Authors' contributions

GQ conceived, designed, and supervised the experiments. ST and BL provided critical discussions. LZ and RT performed the experiments and analyzed the data. LX prepared the strawberry materials. GQ and LZ wrote the manuscript with contributions from RT. All authors read and approved the final manuscript.

Competing interests

The authors declare that they have no competing interests.

Consent for publication

Not applicable.

Ethics approval and consent to participate

Not applicable.

Author details

[1]Key Laboratory of Plant Resources, Institute of Botany, the Innovative Academy of Seed Design, Chinese Academy of Sciences, No.20 Nanxincun, Xiangshan, Haidian District, Beijing 100093, China. [2]University of Chinese Academy of Sciences, Beijing 100049, China. [3]College of Horticulture, China Agricultural University, Beijing 100193, China.

References

1. Wang X, Lu Z, Gomez A, Hon GC, Yue Y, Han D, et al. N^6-methyladenosine dependent regulation of messenger RNA stability. Nature. 2014;505:117-20.
2. Zhao X, Yang Y, Sun BF, Shi Y, Yang X, Xiao W, et al. FTO-dependent demethylation of N^6-methyladenosine regulates mRNA splicing and is required for adipogenesis. Cell Res. 2014;24:1403-19.
3. Wang X, Zhao BS, Roundtree IA, Lu Z, Han D, Ma H, et al. N^6-methyladenosine modulates messenger RNA translation efficiency. Cell. 2015;161:1388-99.
4. Shi H, Wei J, He C. Where, when, and how: context-dependent functions of RNA methylation writers, readers, and erasers. Mol Cell. 2019;74:640-650.
5. Batista PJ, Molinie B, Wang J, Qu K, Zhang J, Li L, et al. m^6A RNA modification controls cell fate transition in mammalian embryonic stem cells. Cell Stem Cell. 2014;15:707-19.
6. Fustin JM, Doi M, Yamaguchi Y, Hida H, Nishimura S, Yoshida M, et al. RNA methylation-dependent RNA processing controls the speed of the circadian clock. Cell. 2013;155:793-806.
7. Lin S, Choe J, Du P, Triboulet R, Gregory RI. The m^6A methyltransferase METTL3 promotes translation in human cancer cells. Mol Cell. 2016;62:335-45.
8. Zhang C, Samanta D, Lu H, Bullen JW, Zhang H, Chen I, et al. Hypoxia induces the breast cancer stem cell phenotype by HIF-dependent and ALKBH5-mediated m^6A-demethylation of NANOG mRNA. Proc Natl Acad Sci U S A. 2016;113:E2047-56.
9. Bertero A, Brown S, Madrigal P, Osnato A, Ortmann D, Yiangou L, et al. The SMAD2/3

873 interactome reveals that TGFβ controls m^{6}A mRNA methylation in pluripotency. Nature.
874 2018;555:256-9.
875 10. Gu C, Shi X, Dai CY, Shen F, Rocco G, Chen JF, et al. RNA m^{6}A modification in cancers:
876 molecular mechanisms and potential clinical applications. The innovation.
877 2020;1:100066.
878 11. Liu J, Yue Y, Han D, Wang X, Fu Y, Zhang L, et al. A METTL3-METTL14 complex
879 mediates mammalian nuclear RNA N^6-adenosine methylation. Nat Chem Biol.
880 2014;10:93-5.
881 12. Wang P, Doxtader KA, Nam Y. Structural basis for cooperative function of METTL3 and
882 METTL14 methyltransferases. Mol Cell. 2016;63:306-17.
883 13. Wang X, Feng J, Xue Y, Guan Z, Zhang D, Liu Z, et al. Structural basis of N^6-adenosine
884 methylation by the METTL3-METTL14 complex. Nature. 2016;534:575-8.
885 14. Ping XL, Sun BF, Wang L, Xiao W, Yang X, Wang WJ, et al. Mammalian WTAP is a
886 regulatory subunit of the RNA N^6-methyladenosine methyltransferase. Cell Res.
887 2014;24:177-89.
888 15. Patil DP, Chen CK, Pickering BF, Chow A, Jackson C, Guttman M, et al. m^{6}A RNA
889 methylation promotes XIST-mediated transcriptional repression. Nature.
890 2016;537:369-73.
891 16. Wen J, Lv R, Ma H, Shen H, He C, Wang J, et al. Zc3h13 regulates nuclear RNA m^{6}A
892 methylation and mouse embryonic stem cell self-renewal. Mol Cell. 2018;69:1028-38.
893 17. Yue Y, Liu J, Cui X, Cao J, Luo G, Zhang Z, et al. VIRMA mediates preferential m^{6}A
894 mRNA methylation in 3' UTR and near stop codon and associates with alternative

895 polyadenylation. Cell Discov. 2018;4:10.

896 18. Jia G, Fu Y, Zhao X, Dai Q, Zheng G, Yang Y, et al. N^6-methyladenosine in nuclear RNA
897 is a major substrate of the obesity-associated FTO. Nat Chem Biol. 2011;7:885-7.

898 19. Zheng G, Dahl JA, Niu Y, Fedorcsak P, Huang CM, Li CJ, et al. ALKBH5 is a
899 mammalian RNA demethylase that impacts RNA metabolism and mouse fertility. Mol
900 Cell. 2013;49:18-29.

901 20. Shen L, Liang Z, Gu X, Chen Y, Teo ZW, Hou X, et al. N^6-methyladenosine RNA
902 modification regulates shoot stem cell fate in Arabidopsis. Dev Cell. 2016;38:186-200.

903 21. Duan HC, Wei LH, Zhang C, Wang Y, Chen L, Lu Z, et al. ALKBH10B is an RNA
904 N^6-methyladenosine demethylase affecting Arabidopsis floral transition. Plant Cell.
905 2017;29:2995-3011.

906 22. Wei LH, Song P, Wang Y, Lu Z, Tang Q, Yu Q, et al. The m^6A reader ECT2 controls
907 trichome morphology by affecting mRNA stability in Arabidopsis. Plant Cell.
908 2018;30:968-85.

909 23. Scutenaire J, Deragon JM, Jean V, Benhamed M, Raynaud C, Favory JJ, et al. The YTH
910 domain protein ECT2 is an m^6A reader required for normal trichome branching in
911 Arabidopsis. Plant Cell. 2018;30:986-1005.

912 24. Zhang F, Zhang YC, Liao JY, Yu Y, Zhou YF, Feng YZ, et al. The subunit of RNA
913 N^6-methyladenosine methyltransferase OsFIP regulates early degeneration of microspores
914 in rice. PLoS Genet. 2019;15:e1008120.

915 25. Miao Z, Zhang T, Qi Y, Song J, Han Z, Ma C. Evolution of the RNA N^6-methyladenosine
916 methylome mediated by genomic duplication. Plant Physiol. 2020;182:345-60.

917 26. Giovannoni JJ, Nguyen C, Ampofo B, Zhong SL, Fei ZJ. The epigenome and
918 transcriptional dynamics of fruit ripening. Annu Rev Plant Biol. 2017;68:61-84.
919 27. Giovannoni JJ. Genetic regulation of fruit development and ripening. Plant Cell.
920 2004;16:S170-80.
921 28. Seymour GB, Østergaard L, Chapman NH, Knapp S, Martin C. Fruit development and
922 ripening. Annu Rev Plant Biol. 2013;64:219-41.
923 29. Matas AJ, Gapper NE, Chung MY, Giovannoni JJ, Rose JK. Biology and genetic
924 engineering of fruit maturation for enhanced quality and shelf-life. Curr Opin Biotechnol.
925 2009;20:197-203.
926 30. Lin Z, Zhong S, Grierson D. Recent advances in ethylene research. J Exp Bot.
927 2009;60:3311-36.
928 31. Li S, Chen K, Grierson D. A critical evaluation of the role of ethylene and MADS
929 transcription factors in the network controlling fleshy fruit ripening. New Phytol.
930 2019;221:1724-41.
931 32. Chen T, Qin G, Tian S. Regulatory network of fruit ripening: current understanding and
932 future challenges. New Phytol. 2020;228:1219-26.
933 33. Liu M, Pirrello J, Chervin C, Roustan JP, Bouzayen M. Ethylene control of fruit ripening:
934 revisiting the complex network of transcriptional regulation. Plant Physiol.
935 2015;169:2380-90.
936 34. Jia HF, Chai YM, Li CL, Lu D, Luo JJ, Qin L, et al. Abscisic acid plays an important role
937 in the regulation of strawberry fruit ripening. Plant Physiol. 2011;157:188-99.
938 35. Tang D, Gallusci P, Lang Z. Fruit development and epigenetic modifications. New Phytol.

939 2020;228:839-44.

940 36. Zhou L, Tian S, Qin G. RNA methylomes reveal the m^6A-mediated regulation of DNA
941 demethylase gene SlDML2 in tomato fruit ripening. Genome Biol. 2019;20:156.

942 37. Dominissini D, Moshitch-Moshkovitz S, Salmon-Divon M, Amariglio N, Rechavi G.
943 Transcriptome-wide mapping of N^6-methyladenosine by m^6A-seq based on
944 immunocapturing and massively parallel sequencing. Nat Protoc. 2013;8:176-89.

945 38. Liao X, Li M, Liu B, Yan M, Yu X, Zi H, et al. Interlinked regulatory loops of ABA
946 catabolism and biosynthesis coordinate fruit growth and ripening in woodland strawberry.
947 Proc Natl Acad Sci U S A. 2018;115:E11542-50.

948 39. Dominissini D, Moshitch-Moshkovitz S, Schwartz S, Salmon-Divon M, Ungar L,
949 Osenberg S, et al. Topology of the human and mouse m^6A RNA methylomes revealed by
950 m6A-seq. Nature. 2012;485:201-6.

951 40. Li Y, Wang X, Li C, Hu S, Yu J, Song S. Transcriptome-wide N^6-methyladenosine
952 profiling of rice callus and leaf reveals the presence of tissue-specific competitors
953 involved in selective mRNA modification. RNA Biol. 2014;11:1180-8.

954 41. Luo GZ, MacQueen A, Zheng G, Duan H, Dore LC, Lu Z, et al. Unique features of the
955 m^6A methylome in Arabidopsis thaliana. Nat Commun. 2014;5:5630.

956 42. Heinz S, Benner C, Spann N, Bertolino E, Lin YC, Laslo P, et al. Simple combinations of
957 lineage-determining transcription factors prime cis-regulatory elements required for
958 macrophage and B cell identities. Mol Cell. 2010;38:576–89.

959 43. Meyer KD, Saletore Y, Zumbo P, Elemento O, Mason CE, Jaffrey SR. Comprehensive
960 analysis of mRNA methylation reveals enrichment in 3' UTRs and near stop codons. Cell.

961 2012;149:1635–46.

962 44. Wan YZ, Tang K, Zhang DY, Xie SJ, Zhu XH, Wang Z, et al. Transcriptome-wide
963 high-throughput deep m^6A-seq reveals unique differential m^6A methylation patterns
964 between three organs in Arabidopsis thaliana. Genome Biol. 2015;16:272.

965 45. Fujii H, Chinnusamy V, Rodrigues A, Rubio S, Antoni R, Park SY, et al. In vitro
966 reconstitution of an abscisic acid signaling pathway. Nature. 2009;462:660-4.

967 46. Furihata T, Maruyama K, Fujita Y, Umezawa T, Yoshida R, Shinozaki K, et al. Abscisic
968 acid-dependent multisite phosphorylation regulates the activity of a transcription activator
969 AREB1. Proc Natl Acad Sci U S A. 2006;103:1988-93.

970 47. Shang Y, Yan L, Liu ZQ, Cao Z, Mei C, Xin Q, et al. The Mg-chelatase H subunit of
971 Arabidopsis antagonizes a group of WRKY transcription repressors to relieve
972 ABA-responsive genes of inhibition. Plant Cell. 2010;22:1909-35.

973 48. Bai Q, Huang Y, Shen Y. The physiological and molecular mechanism of abscisic acid in
974 regulation of fleshy fruit ripening. Front Plant Sci. 2021;11:619953.

975 49. Merchante C, Brumos J, Yun J, Hu Q, Spencer KR, Enríquez P, et al. Gene-specific
976 translation regulation mediated by the hormone-signaling molecule EIN2. Cell.
977 2015;163:684-97.

978 50. Liang Z, Riaz A, Chachar S, Ding Y, Du H, Gu X. Epigenetic modifications of mRNA
979 and DNA in plants. Mol Plant. 2020;13:14-30.

980 51. Zhong S, Li H, Bodi Z, Button J, Vespa L, Herzog M, et al. MTA is an Arabidopsis
981 messenger RNA adenosine methylase and interacts with a homolog of a sex-specific
982 splicing factor. Plant Cell. 2008;20:1278-88.

983 52. Ruzicka K, Zhang M, Campilho A, Bodi Z, Kashif M, Saleh M, et al. Identification of
984 factors required for m^6A mRNA methylation in Arabidopsis reveals a role for the
985 conserved E3 ubiquitin ligase HAKAI. New Phytol. 2017;215:157-72.
986 53. Hoffmann T, Kalinowski G, Schwab W. RNAi-induced silencing of gene expression in
987 strawberry fruit (*Fragaria* × *ananassa*) by agroinfiltration: a rapid assay for gene
988 function analysis. Plant J. 2006;48:818-26.
989 54. Cheng JF, Niu QF, Zhang B, Chen KS, Yang RH, Zhu JK, et al. Downregulation of
990 RdDM during strawberry fruit ripening. Genome Biol. 2018;19:212.
991 55. Chen K, Li GJ, Bressan RA, Song CP, Zhu JK, Zhao Y. Abscisic acid dynamics, signaling,
992 and functions in plants. J Integr Plant Biol. 2020;62:25-54.
993 56. Chai YM, Jia HF, Li CL, Dong QH, Shen YY. FaPYR1 is involved in strawberry fruit
994 ripening. J Exp Bot. 2011;62:5079-89.
995 57. Jia HF, Lu D, Sun JH, Li CL, Xing Y, Qin L, et al. Type 2C protein phosphatase ABI1 is a
996 negative regulator of strawberry fruit ripening. J Exp Bot. 2013;64:1677-87.
997 58. Han Y, Dang R, Li J, Jiang J, Zhang N, Jia M, et al. SUCROSE
998 NONFERMENTING1-RELATED PROTEIN KINASE2.6, an ortholog of OPEN
999 STOMATA 1, is a negative regulator of strawberry fruit development and ripening. Plant
1000 Physiol. 2015;167:915-30.
1001 59. Wang K, He J, Zhao Y, Wu T, Zhou X, Ding Y, et al. EAR1 negatively regulates ABA
1002 signaling by enhancing 2C protein phosphatase activity. Plant Cell. 2018;30:815-34.
1003 60. Castillo MC, Lozano□Juste J, González□Guzmán M, Rodriguez L, Rodriguez PL, León
1004 J. Inactivation of PYR/PYL/RCAR ABA receptors by tyrosine nitration may enable rapid

1005 inhibition of ABA signaling by nitric oxide in plants. Sci Signal. 2015;8:ra89.
1006 61. Irigoyen ML, Iniesto E, Rodriguez L, Puga MI, Yanagawa Y, Pick E, et al. Targeted
1007 degradation of abscisic acid receptors is mediated by the ubiquitin ligase substrate adaptor
1008 DDA1 in Arabidopsis. Plant Cell. 2014;26:712-28.
1009 62. Umezawa T, Sugiyama N, Mizoguchi M, Hayashi S, Myouga F, Yamaguchi□Shinozaki K,
1010 et al. Type 2C protein phosphatases directly regulate abscisic acid□activated protein
1011 kinases in Arabidopsis. Proc Natl Acad Sci U S A. 2009;106:17588-93.
1012 63. Umezawa T, Sugiyama N, Takahashi F, Anderson JC, Ishihama Y, Peck SC, et al.
1013 Genetics and phosphoproteomics reveal a protein phosphorylation network in the abscisic
1014 acid signaling pathway in Arabidopsis thaliana. Sci Signal. 2013;6:rs8.
1015 64. Cai Z, Liu J, Wang H, Yang C, Chen Y, Li Y, et al. GSK3□like kinases positively
1016 modulate abscisic acid signaling through phosphorylating subgroup III SnRK2s in
1017 Arabidopsis. Proc Natl Acad Sci U S A. 2014;111:9651-6.
1018 65. Shinozawa A, Otake R, Takezawa D, Umezawa T, Komatsu K, Tanaka K, et al. SnRK2
1019 protein kinases represent an ancient system in plants for adaptation to a terrestrial
1020 environment. Commun Biol. 2019;2:30.
1021 66. Bhaskara GB, Nguyen TT, Verslues P. Unique drought resistance functions of the highly
1022 ABA-induced clade A protein phosphatase 2Cs. Plant Physiol. 2012;160: 379-95.
1023 67. Tan W, Zhang D, Zhou H, Zheng T, Yin Y, Lin H. Transcription factor HAT1 is a substrate
1024 of SnRK2.3 kinase and negatively regulates ABA synthesis and signaling in Arabidopsis
1025 responding to drought. PLoS Genet. 2018;14:e10073363.
1026 68. Liu S, Kracher B, Ziegler J, Birkenbihl RP, Somssich IE. Negative regulation of ABA

1027 signaling by WRKY33 is critical for Arabidopsis immunity towards Botrytis cinerea 2100.
1028 eLife. 2015;4:e07295.
1029 69. Meyer KD, Patil DP, Zhou J, Zinoviev A, Skabkin MA, Elemento O, et al. 5' UTR m^6A
1030 promotes cap-independent translation. Cell. 2015;163:999-1010.
1031 70. Huang H, Weng H, Sun W, Qin X, Shi H, Wu H, et al. Recognition of RNA
1032 N^6-methyladenosine by IGF2BP proteins enhances mRNA stability and translation. Nat
1033 Cell Biol. 2018;20:285-95.
1034 71. Guo J, Wang S, Yu X, Dong R, Li Y, Mei X, et al. Polyamines regulate strawberry fruit
1035 ripening by abscisic acid, auxin, and ethylene. Plant Physiol. 2018;177:339-51.
1036 72. Martin M. Cutadapt removes adapter sequences from high-throughput sequencing reads.
1037 EMBnet J. 2011;17:10-2.
1038 73. Bolger AM, Lohse M, Usadel B. Trimmomatic: a flexible trimmer for Illumina sequence
1039 data. Bioinformatics. 2014;30:2114-20.
1040 74. Li H, Durbin R. Fast and accurate short read alignment with Burrows Wheeler transform.
1041 Bioinformatics. 2009;25:1754-60.
1042 75. Zhang Y, Liu T, Meyer AC, Eeckhoute J, Johnson DS, Bernstein BE, et al. Model-based
1043 analysis of ChIP-seq (MACS). Genome Biol. 2008;9:R137.
1044 76. Salmon-Divon M, Dvinge H, Tammoja K, Bertone P. PeakAnalyzer: genome-wide
1045 annotation of chromatin binding and modification loci. Bioinformatics. 2010;11:415.
1046 77. Meng J, Cui X, Liu H, Zhang L, Zhang S, Rao MK, et al. Unveiling the dynamics in RNA
1047 epigenetic regulations. In: 2013 IEEE International Conference on Bioinformatics and
1048 Biomedicine (BIBM). 2013;139-44.

78. Heinz S, Benner C, Spann N, Bertolino E, Lin YC, Laslo P, et al. Simple combinations of lineage-determining transcription factors prime cis-regulatory elements required for macrophage and B cell identities. Mol Cell. 2010;38:576-89.

79. Nicol JW, Helt GA, Blanchard SG, Raja A, Loraine AE. The Integrated Genome Browser: free software for distribution and exploration of genome-scale datasets. Bioinformatics. 2009;25:2730-1.

80. Tian T, Liu Y, Yan HY, You Q, Yi X, Du Z, et al. agriGO v2.0: a GO analysis toolkit for the agricultural community, 2017 update. Nucleic Acids Res. 2017;gkx382.

81. Trapnell C, Williams BA, Pertea G, Mortazavi A, Kwan G, van Baren MJ, et al. Transcript assembly and quantification by RNA-seq reveals unannotated transcripts and isoform switching during cell differentiation. Nat Biotechnol. 2010;28:511-5.

82. Benjamini Y, Hochberg Y. Controlling the false discovery rate: a practical and powerful approach to multiple testing. J Roy Stat Soc B. 1995;57:289-300.

83. Schmittgen TD, Livak KJ. Analyzing real-time PCR data by the comparative C(T) method. Nat Protoc. 2008;3:1101-8.

84. Xu K, Yang Y, Feng GH, Sun BF, Chen JQ, Li YF, et al. METTL3-mediated m^6A regulates spermatogonial differentiation and meiosis initiation. Cell Res. 2017;27:1100-14.

85. Mistry J, Finn RD, Eddy SR, Bateman A, Punta M. Challenges in homology search: HMMER3 and convergent evolution of coiled-coil regions. Nucleic Acids Res. 2013;41:e121.

86. Marchler-Bauer A, Derbyshire MK, Gonzales NR, Lu S, Chitsaz F, Geer LY, et al. CDD:

1071 NCBI's conserved domain database. Nucleic Acids Res. 2015;43:D222-6.

1072 87. Larkin MA, Blackshields G, Brown NP, Chenna R, McGettigan PA, McWilliam H, et al.
1073 Clustal W and Clustal X version 2.0. Bioinformatics. 2007;23:2947-8.

1074 88. Tamura K, Peterson D, Peterson N, Stecher G, Nei M, Kumar S. MEGA5: molecular
1075 evolutionary genetics analysis using maximum likelihood, evolutionary distance, and
1076 maximum parsimony methods. Mol Biol Evol. 2011;28:2731-9.

1077 89. Wang P, Wang Y, Wang W, Chen T, Tian S, Qin G. Ubiquitination of phytoene synthase 1
1078 precursor modulates carotenoid biosynthesis in tomato. Commun Biol. 2020;3:730.

1079 90. Chen H, Zou Y, Shang Y, Lin H, Wang Y, Cai R, et al. Firefly luciferase complementation
1080 imaging assay for protein-protein interactions in plants. Plant Physiol. 2008;146:368-76.

1081 91. Lei R, Qiao W, Hu F, Jiang H, Zhu S. A simple and effective method to encapsulate
1082 tobacco mesophyll protoplasts to maintain cell viability. MethodsX. 2014;2:24-32.

1083 92. Zhou LL, Tang RK, Li XJ, Tian SP, Li BB, Qin GZ. N^6-methyladenosine RNA
1084 modification regulates strawberry fruit ripening in an ABA-dependent manner. Genome
1085 biol. 2021.

1086

Figure legends

Figure 1 Transcriptome-wide m^{6}A methylomes in strawberry fruit. a The representative photographs of fruit at different developmental stages. S6, the growth stage 6; RS1, the ripening stage 1; RS3, the ripening stage 3. Scale bar = 1 cm. **b** Venn diagrams depicting the overlap of m^{6}A peaks from three independent m^{6}A-seq experiments on fruit at the three developmental stages. Rep, replicate. **c** Percentage of the m^{6}A-containing transcripts containing various m^{6}A peak numbers among samples. **d** Gene Ontology (GO) enrichment for the m^{6}A-modified transcripts identified in m^{6}A-seq.

Figure 2 Dynamic distribution of m^{6}A during strawberry fruit ripening. a Metagenomic profiles of m^{6}A peak summit distribution along transcripts. UTR, untranslated region; CDS, coding sequence. The red arrows indicate the changes in m^{6}A distribution in the CDS region adjacent to the start codon in the ripening process, while the green arrows show the changes in m^{6}A distribution around the stop codon or within the 3' UTR. S6, the growth stage 6; RS1, the ripening stage 1; RS3, the ripening stage 3. **b** and **c** The percentage (**b**) and relative enrichment (**c**) of m^{6}A peak summits in five non-overlapping transcript segments. TSS, transcription start site.

Figure 3 Correlation between m^{6}A modification and mRNA abundance in strawberry fruit. a Scatter plots showing hypermethylated (red) and hypomethylated (blue) m^{6}A peaks in fruit at RS1 stage compared to those at S6 stage. S6, the growth stage 6; RS1, the ripening stage 1. **b** Scatter plots depicting hypermethylated (red) and hypomethylated (blue) m^{6}A

peaks in fruit at RS3 stage compared to those at RS1 stage. RS3, the ripening stage 3. **c** and **d** The distribution characteristics of the differential m^6A peaks shown in **a** (**c**) and **b** (**d**). TSS, transcription start site; UTR, untranslated region; CDS, coding sequence. **e** and **f** Scatter plots displaying the expression of transcripts containing hypermethylated (**e**) or hypomethylated (**f**) m^6A peaks shown in **a**. Transcripts with significantly higher and lower levels (fold change ≥ 1.5; *P* value < 0.05) in fruit at RS1 stage compared to those at S6 stage are highlighted in red and blue, respectively. **g** and **h** Scatter plots showing the expression of transcripts harboring hypermethylated (**g**) or hypomethylated (**h**) m^6A peaks shown in **b**. Transcripts with significantly higher and lower levels (fold change ≥ 1.5; *P* value < 0.05) in fruit at RS3 stage compared to those at RS1 stage are highlighted in red and blue, respectively. **i** Gene expression ratios based on the distributions of differential m^6A peaks between fruit at RS1 and S6 stages. **j** Scatter plots exhibiting the expression of transcripts concurrently containing hypermethylated m^6A peaks in the CDS region and hypomethylated m^6A peaks around the stop codon or within the 3' UTR in fruit at RS1 stage compared to those at S6 stage. Transcripts with significantly higher and lower levels (fold change ≥ 1.5; *P* value < 0.05) in fruit at RS1 stage compared to those at S6 stage are highlighted in red and blue, respectively. Gene expression analysis in **e**-**j** was performed by RNA-seq. FPKM, fragments per kilobase of exon per million mapped fragments.

Figure 4 m^6A modification facilitates mRNA stability or translation of genes in ABA pathway. a A brief model of the two core ABA signaling pathways in plants. **b** Integrated Genome Browser (IGB) tracks showing the distribution of m^6A reads in transcripts of the

9-cis-epoxycarotenoid dioxygenase 5 (*NCED5*), *putative ABA receptor* (*ABAR*), and *ABA-responsive element-binding protein 1* (*AREB1*). The hypermethylated m^6A peaks (fold change ≥ 1.5; *P* value < 0.05) in fruit at RS1 stage compared to those at S6 stage are indicated by shadow boxes. S6, the growth stage 6; RS1, the ripening stage 1. Rep, replicate. **c** m^6A enrichment for *NCED5*, *ABAR*, and *AREB1* from m^6A-seq data. **d** Validations of the m^6A enrichment by m^6A-immunoprecipitation (IP)-qPCR. **e** and **f** Transcript levels of *NCED5*, *ABAR*, and *AREB1* determined by RNA-seq (**e**) and quantitative RT-PCR (**f**). FPKM, fragments per kilobase of exon per million mapped fragments. The *ACTIN* gene served as an internal control in f. **g** Schematic diagram of the expression cassettes used for mRNA stability assay. The intact (WT) or mutated (MU) cDNA fragments of *NCED5*, *ABAR*, and *AREB1* were separately cloned into the pCambia2300 vector driven by the CaMV 35S promoter. The potential m^6A sites identified in m^6A-seq were mutated from adenosine (A) to cytidine (C) or guanine (G) using site-directed mutagenesis kit. **h** Determination of mRNA stability for *NCED5*, *ABAR*, and *AREB1*. The intact (WT) or mutated (MU) cDNA fragments were expressed in *Nicotiana benthamiana* leaves. After actinomycin D treatment at an indicated time point, the total RNAs were extracted and submitted to quantitative RT-PCR assay with the *N. benthamiana ACTIN* gene serving as an internal control. **i** m^6A-IP-qPCR assay showing the relative m^6A enrichment in the intact or mutated transcripts. **j** Brief workflow for analysis of translation efficiency. **k** Translation efficiency of *NCED5*, *ABAR*, and *AREB1*. Translation efficiency was expressed as the abundance ratio of mRNA in the polysomal RNA versus the total RNA. Data are presented as mean ± standard deviation (n = 3). Asterisks indicate significant differences (*P < 0.05, **P < 0.01, ***P < 0.001; Student's t test).

Figure 5 The m^{6}A methyltransferase MTA interacts with MTB in strawberry. a The working model for m^{6}A installations mediated by the methyltransferase complex in mammals. The m^{6}A methyltransferases METTL3 and METTL14 interact and function as the stable catalytic core for internal m^{6}A installations in the form of heterodimer. **b** Phylogenetic analysis of eukaryotic m^{6}A methyltransferases. The phylogenetic tree was generated by MEGA (version 5.2). Bootstrap values from 1000 replications for each branch are presented. Species names are abbreviated as follows: Hs, *Homo sapiens*; Ms, *Mus musculus*; At, *Arabidopsis thaliana*; Os, *Oryza sativa*; Zm, *Zea mays*; Sl, *Solanum lycopersicum*; Nb, *Nicotiana benthamiana*; Fa, *Fragaria* × *ananassa*; Fve, *Fragaria vesca*. **c** Transcript levels of the m^{6}A methyltransferase genes *MTA* and *MTB* in diploid woodland strawberry at different developmental stages revealed by RNA-seq. S6, the growth stage 6; RS1, the ripening stage 1; RS3, the ripening stage 3. **d** Representative images of octoploid cultivated strawberry fruit at various developmental stages. SG, small green; Wt, white; IR, initial red; FR, full red. Scale bar = 1 cm. **e** Transcript levels of *MTA* and *MTB* in octoploid strawberry fruit determined by quantitative RT-PCR. The *ACTIN* gene was used as an internal control. Data are presented as mean ± standard deviation (n = 3). Asterisks indicate significant differences (*P < 0.05, **P < 0.01, ***P < 0.001; Student's t test). **f** Y2H assay revealing the interactions between MTA and MTB. The MTA fused with the activation domain (AD) of GAL4 (AD-MTA) and the MTB fused with the binding domain (BD) of GAL4 (BD-MTB) were co-expressed in yeast. The transformants were grew on SD/-Leu/-Trp (-LW), and further selected on SD/-Leu/-Trp/-His (-LWH) and SD/-Leu/-Trp/-His/-Ade (-LWHA) with or

without X-α-gal. **g** LCI assay revealing the interactions between MTA and MTB. The MTA fused with the N-terminus of LUC (MTA-nLUC) was co-expressed with the MTB or its MT-A70 domain fused with the C-terminus of LUC (cLUC-MTB or cLUC-MTB^{D}) in *N. benthamiana* leaves. **h** and **i** Subcellular localization (**h**) and colocalization (**i**) of MTA and MTB. The MTA-mCherry or/and MTB-eGFP fusion proteins were transiently expressed into *N. benthamiana* leaves. The *N. benthamiana* leaves expressing eGFP or/and mCherry were used as the negative control. Scale bar = 10 μm.

Figure 6 m^{6}A methyltransferases positively regulate the ripening of strawberry fruit. a Ripening phenotypes of MTA/MTB RNA interference (RNAi-MTA/RNAi-MTB) and overexpression (OE-MTA/OE-MTB) fruits. Strawberry fruit agroinfiltrated with empty plasmid were used as controls. The representative images are shown. Scale bar = 1 cm. **b** Transcript levels of *MTA* and *MTB*, as well as the two important ripening genes *CHS* and *PG1*, in the RNAi and overexpression fruits determined by quantitative RT-PCR. The *ACTIN* gene served as an internal control. **c** LC-MS/MS assay revealing the changes in global m^{6}A methylation levels in the MTA-overexpressed fruits. **d** RNA immunoprecipitation (RIP) assay revealing the binding of MTA protein to the transcripts of *NCED5*, *ABAR*, and *AREB1*. The protein-RNA complexes were extracted from strawberry fruit expressing the MTA-eGFP fusion protein and subjected to immunoprecipitation with anti-GFP monoclonal antibody or mouse IgG (negative control). **e**-**h** The changes in relative m^{6}A enrichment (**e**), gene expression (**f**), mRNA stability (**g**), and translation efficiency (**h**) of *NCED5*, *ABAR*, and *AREB1* in the MTA-overexpressed fruits. The relative m^{6}A enrichment and gene expression

were determined by m^{6}A-IP-qPCR and quantitative RT-PCR, respectively. For mRNA stability assay, the total RNAs were extracted after actinomycin D treatment at an indicated time point and submitted to quantitative RT-PCR assay. Translation efficiency was expressed as the abundance ratio of mRNA in the polysomal RNA versus the total RNA. Data are presented as mean ± standard deviation (n = 3). Asterisks indicate significant differences (*P < 0.05, **P < 0.01, ***P < 0.001; Student's t test). NS, no significance.

Figure 7 Influence of m^{6}A on translation initiation factors or elongation factors in strawberry. a Integrated Genome Browser (IGB) tracks displaying the distribution of m^{6}A reads in transcripts of genes encoding translation initiation factors (*EIF2*, *EIF2B*, *EIF3A*, and *EIF3C*) and elongation factors (*EF1A*). The hypermethylated m^{6}A peaks (fold change ≥ 1.5; P value < 0.05) in fruit at RS1 stage compared to those at S6 stage are indicated by shadow boxes. S6, the growth stage 6; RS1, the ripening stage 1. Rep, replicate. **b** m^{6}A enrichment for *EIF2*, *EIF2B*, *EIF3A*, *EIF3C*, and *EF1A* from m^{6}A-seq data. **c** Transcript levels of *EIF2*, *EIF2B*, *EIF3A*, *EIF3C*, and *EF1A* determined by RNA-seq. FPKM, fragments per kilobase of exon per million mapped fragments. **d** and **e** Relative m^{6}A enrichment (**d**) and gene expression (**e**) for *EIF2*, *EIF2B*, *EIF3A*, *EIF3C*, and *EF1A* in the octoploid strawberry fruit at the white (Wt) and initial red (IR) stages. The relative m^{6}A enrichment and gene expression were determined by m^{6}A-IP-qPCR and quantitative RT-PCR, respectively. The *ACTIN* gene served as an internal control. **f** RNA immunoprecipitation (RIP) assay revealing the binding of MTA protein to the transcripts of *EIF2*, *EIF2B*, *EIF3A*, *EIF3C*, and *EF1A*. **g-i** The changes in relative m^{6}A enrichment (**g**), gene expression (**h**), and mRNA stability (**i**), of *EIF2*, *EIF2B*,

1219 *EIF3A*, *EIF3C*, and *EF1A* in the MTA-overexpressed fruits. For mRNA stability assay, the
1220 total RNAs were extracted after actinomycin D treatment at an indicated time point and
1221 subjected to quantitative RT-PCR assay. Data are presented as mean ± standard deviation (n =
1222 3). Asterisks indicate significant differences (*$P < 0.05$, **$P < 0.01$, ***$P < 0.001$; Student's
1223 t test).
1224

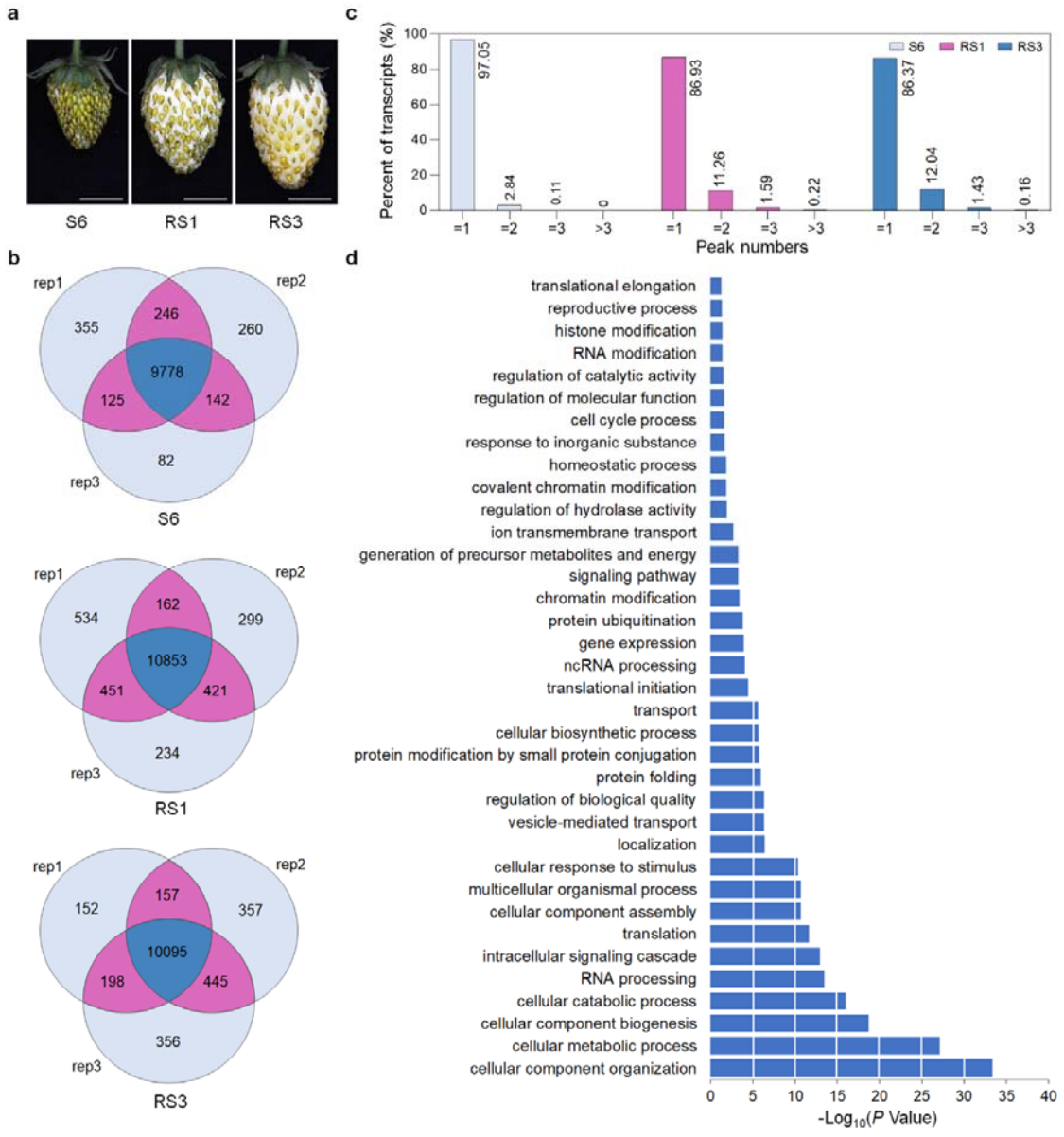

Figure 1 Transcriptome-wide m^{6}A methylomes in strawberry fruit. a The representative photographs of fruit at different developmental stages. S6, the growth stage 6; RS1, the ripening stage 1; RS3, the ripening stage 3. Scale bar = 1 cm. **b** Venn diagrams depicting the overlap of m^{6}A peaks from three independent m^{6}A-seq experiments on fruit at the three developmental stages. Rep, replicate. **c** Percentage of the m^{6}A-containing transcripts containing various m^{6}A peak numbers among samples. **d** Gene Ontology (GO) enrichment for the m^{6}A-modified transcripts identified in m^{6}A-seq.

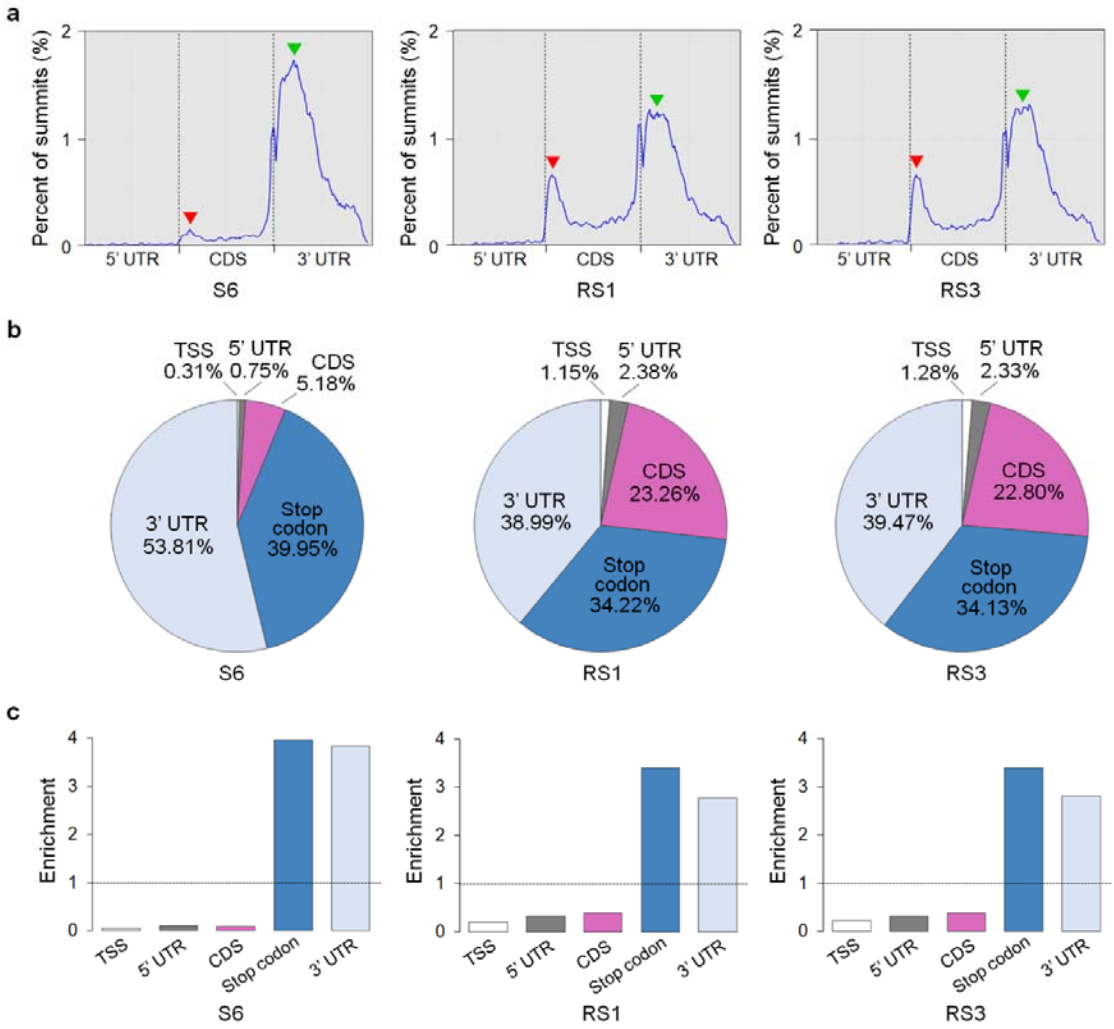

Figure 2 Dynamic distribution of m^{6}A during strawberry fruit ripening. a Metagenomic profiles of m^{6}A peak summit distribution along transcripts. UTR, untranslated region; CDS, coding sequence. The red arrows indicate the changes in m^{6}A distribution in the CDS region adjacent to the start codon in the ripening process, while the green arrows show the changes in m^{6}A distribution around the stop codon or within the 3' UTR. S6, the growth stage 6; RS1, the ripening stage 1; RS3, the ripening stage 3. **b** and **c** The percentage (**b**) and relative enrichment (**c**) of m^{6}A peak summits in five non-overlapping transcript segments. TSS, transcription start site.

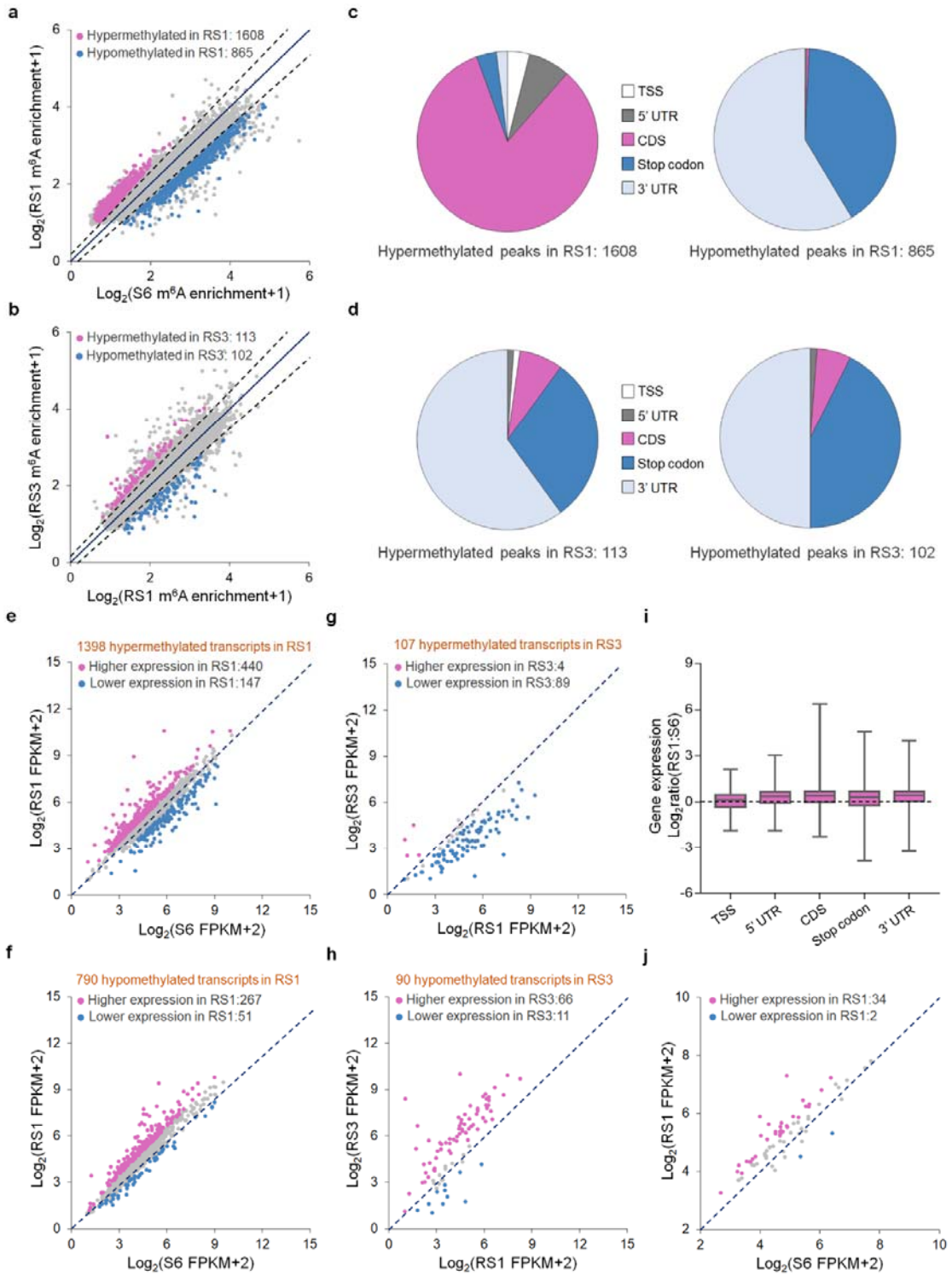

Figure 3 Correlation between m^{6}A modification and mRNA abundance in strawberry fruit. a Scatter plots showing hypermethylated (red) and hypomethylated (blue) m^{6}A peaks in fruit at RS1 stage compared to those at S6 stage. S6, the growth stage 6; RS1, the ripening stage 1. **b** Scatter plots depicting hypermethylated (red) and hypomethylated (blue) m^{6}A peaks in fruit at RS3 stage compared to those at RS1 stage. RS3, the ripening stage 3. **c** and **d** The distribution characteristics of the

differential m^6A peaks shown in **a** (**c**) and **b** (**d**). TSS, transcription start site; UTR, untranslated region; CDS, coding sequence. **e** and **f** Scatter plots displaying the expression of transcripts containing hypermethylated (**e**) or hypomethylated (**f**) m^6A peaks shown in **a**. Transcripts with significantly higher and lower levels (fold change ≥ 1.5; *P* value < 0.05) in fruit at RS1 stage compared to those at S6 stage are highlighted in red and blue, respectively. **g** and **h** Scatter plots showing the expression of transcripts harboring hypermethylated (**g**) or hypomethylated (**h**) m^6A peaks shown in **b**. Transcripts with significantly higher and lower levels (fold change ≥ 1.5; *P* value < 0.05) in fruit at RS3 stage compared to those at RS1 stage are highlighted in red and blue, respectively. **i** Gene expression ratios based on the distributions of differential m^6A peaks between fruit at RS1 and S6 stages. **j** Scatter plots exhibiting the expression of transcripts concurrently containing hypermethylated m^6A peaks in the CDS region and hypomethylated m^6A peaks around the stop codon or within the 3' UTR in fruit at RS1 stage compared to those at S6 stage. Transcripts with significantly higher and lower levels (fold change ≥ 1.5; *P* value < 0.05) in fruit at RS1 stage compared to those at S6 stage are highlighted in red and blue, respectively. Gene expression analysis in **e-j** was performed by RNA-seq. FPKM, fragments per kilobase of exon per million mapped fragments.

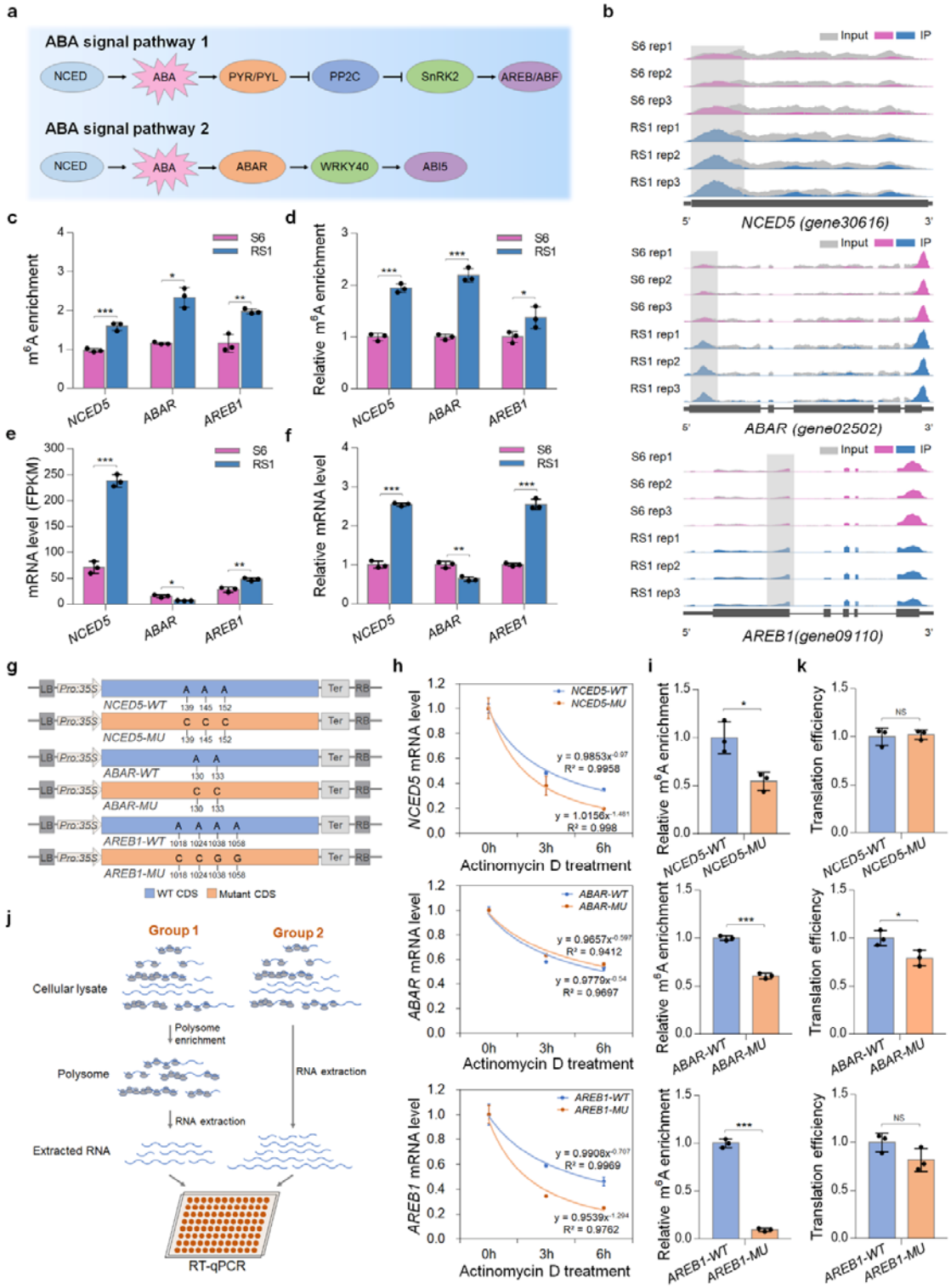

Figure 4 m^{6}A modification facilitates mRNA stability or translation of genes in ABA pathway. a A brief model of the two core ABA signaling pathways in plants. **b** Integrated Genome Browser (IGB) tracks showing the distribution of m^{6}A reads in transcripts of the *9-cis-epoxycarotenoid dioxygenase 5* (*NCED5*), *putative ABA receptor* (*ABAR*), and *ABA-responsive element-binding protein 1* (*AREB1*).

The hypermethylated m^{6}A peaks (fold change ≥ 1.5; *P* value < 0.05) in fruit at RS1 stage compared to those at S6 stage are indicated by shadow boxes. S6, the growth stage 6; RS1, the ripening stage 1. Rep, replicate. **c** m^{6}A enrichment for *NCED5*, *ABAR*, and *AREB1* from m^{6}A-seq data. **d** Validations of the m^{6}A enrichment by m^{6}A-immunoprecipitation (IP)-qPCR. **e** and **f** Transcript levels of *NCED5*, *ABAR*, and *AREB1* determined by RNA-seq (**e**) and quantitative RT-PCR (**f**). FPKM, fragments per kilobase of exon per million mapped fragments. The *ACTIN* gene served as an internal control in f. **g** Schematic diagram of the expression cassettes used for mRNA stability assay. The intact (WT) or mutated (MU) cDNA fragments of *NCED5*, *ABAR*, and *AREB1* were separately cloned into the pCambia2300 vector driven by the CaMV 35S promoter. The potential m^{6}A sites identified in m^{6}A-seq were mutated from adenosine (A) to cytidine (C) or guanine (G) using site-directed mutagenesis kit. **h** Determination of mRNA stability for *NCED5*, *ABAR*, and *AREB1*. The intact (WT) or mutated (MU) cDNA fragments were expressed in *Nicotiana benthamiana* leaves. After actinomycin D treatment at an indicated time point, the total RNAs were extracted and submitted to quantitative RT-PCR assay with the *N. benthamiana ACTIN* gene serving as an internal control. **i** m^{6}A-IP-qPCR assay showing the relative m^{6}A enrichment in the intact or mutated transcripts. **j** Brief workflow for analysis of translation efficiency. **k** Translation efficiency of *NCED5*, *ABAR*, and *AREB1*. Translation efficiency was expressed as the abundance ratio of mRNA in the polysomal RNA versus the total RNA. Data are presented as mean ± standard deviation (n = 3). Asterisks indicate significant differences (**P* < 0.05, ***P* < 0.01, ****P* < 0.001; Student's t test).

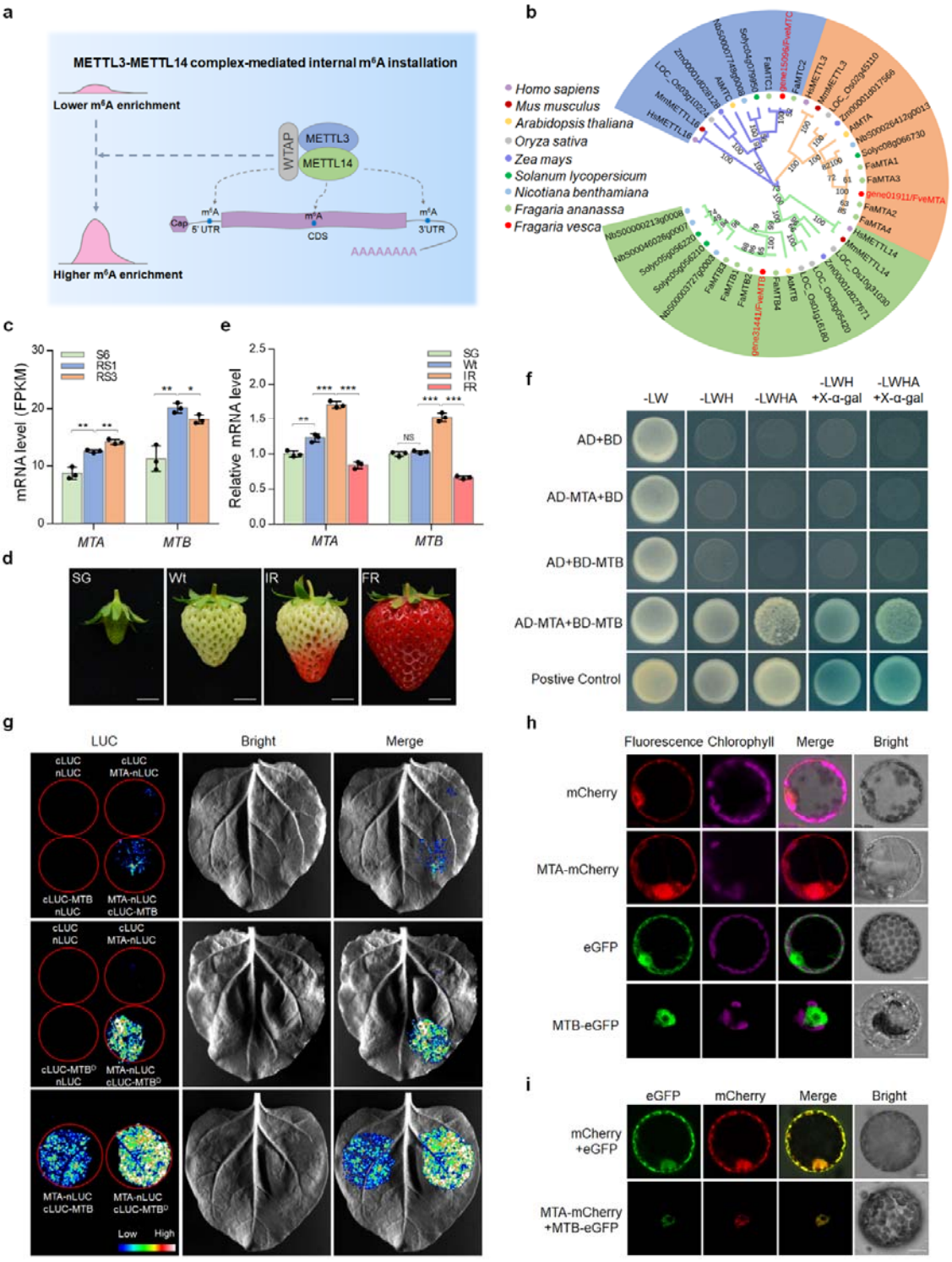

Figure 5 The m^{6}A methyltransferase MTA interacts with MTB in strawberry. a The working model for m^{6}A installations mediated by the methyltransferase complex in mammals. The m^{6}A methyltransferases METTL3 and METTL14 interact and function as the stable catalytic core for internal m^{6}A installations in the form of heterodimer. **b** Phylogenetic analysis of eukaryotic m^{6}A methyltransferases. The phylogenetic tree was generated by MEGA (version 5.2). Bootstrap values

from 1000 replications for each branch are presented. Species names are abbreviated as follows: Hs, *Homo sapiens*; Ms, *Mus musculus*; At, *Arabidopsis thaliana*; Os, *Oryza sativa*; Zm, *Zea mays*; Sl, *Solanum lycopersicum*; Nb, *Nicotiana benthamiana*; Fa, *Fragaria* × *ananassa*; Fve, *Fragaria vesca*. **c** Transcript levels of the m^6A methyltransferase genes *MTA* and *MTB* in diploid woodland strawberry at different developmental stages revealed by RNA-seq. S6, the growth stage 6; RS1, the ripening stage 1; RS3, the ripening stage 3. **d** Representative images of octoploid cultivated strawberry fruit at various developmental stages. SG, small green; Wt, white; IR, initial red; FR, full red. Scale bar = 1 cm. **e** Transcript levels of *MTA* and *MTB* in octoploid strawberry fruit determined by quantitative RT-PCR. The *ACTIN* gene was used as an internal control. Data are presented as mean ± standard deviation (n = 3). Asterisks indicate significant differences (*P < 0.05, **P < 0.01, ***P < 0.001; Student's t test). **f** Y2H assay revealing the interactions between MTA and MTB. The MTA fused with the activation domain (AD) of GAL4 (AD-MTA) and the MTB fused with the binding domain (BD) of GAL4 (BD-MTB) were co-expressed in yeast. The transformants were grew on SD/-Leu/-Trp (-LW), and further selected on SD/-Leu/-Trp/-His (-LWH) and SD/-Leu/-Trp/-His/-Ade (-LWHA) with or without X-α-gal. **g** LCI assay revealing the interactions between MTA and MTB. The MTA fused with the N-terminus of LUC (MTA-nLUC) was co-expressed with the MTB or its MT-A70 domain fused with the C-terminus of LUC (cLUC-MTB or cLUC-MTB^D) in *N. benthamiana* leaves. **h** and **i** Subcellular localization (**h**) and colocalization (**i**) of MTA and MTB. The MTA-mCherry or/and MTB-eGFP fusion proteins were transiently expressed into *N. benthamiana* leaves. The *N. benthamiana* leaves expressing eGFP or/and mCherry were used as the negative control. Scale bar = 10 μm.

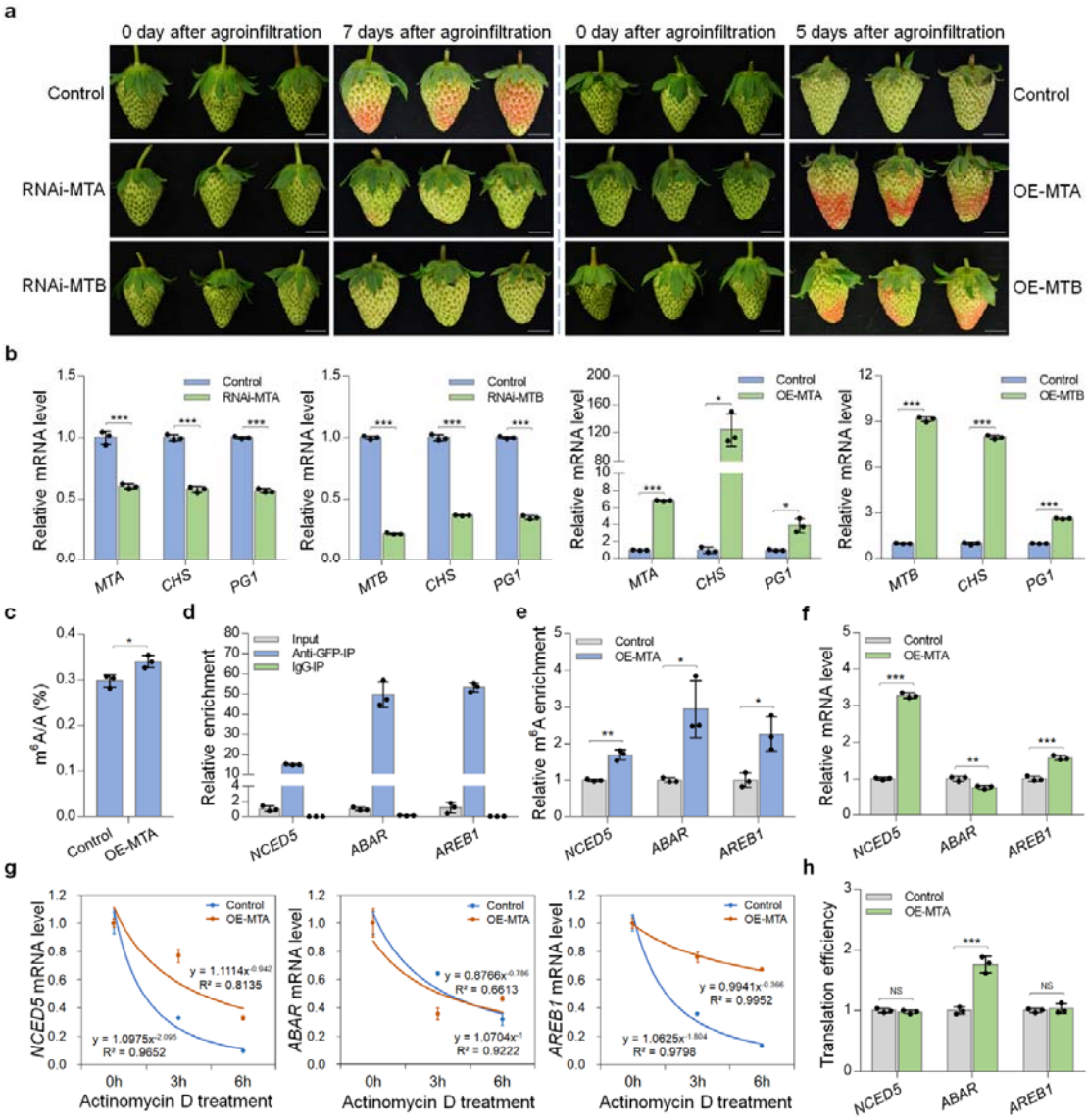

Figure 6 m^{6}A methyltransferases positively regulate the ripening of strawberry fruit. a Ripening phenotypes of MTA/MTB RNA interference (RNAi-MTA/RNAi-MTB) and overexpression (OE-MTA/OE-MTB) fruits. Strawberry fruit agroinfiltrated with empty plasmid were used as controls. The representative images are shown. Scale bar = 1 cm. **b** Transcript levels of *MTA* and *MTB*, as well as the two important ripening genes *CHS* and *PG1*, in the RNAi and overexpression fruits determined by quantitative RT-PCR. The *ACTIN* gene served as an internal control. **c** LC-MS/MS assay revealing the changes in global m^{6}A methylation levels in the MTA-overexpressed fruits. **d** RNA immunoprecipitation (RIP) assay revealing the binding of MTA protein to the transcripts of *NCED5*, *ABAR*, and *AREB1*. The protein-RNA complexes were extracted from strawberry fruit expressing the MTA-eGFP fusion protein and subjected to immunoprecipitation with anti-GFP monoclonal antibody or mouse IgG (negative control). **e**-**h** The changes in relative m^{6}A enrichment (**e**), gene expression (**f**), mRNA stability (**g**), and translation efficiency (**h**) of *NCED5*, *ABAR*, and *AREB1* in the MTA-overexpressed fruits. The relative m^{6}A enrichment and gene expression were determined by m^{6}A-IP-qPCR and quantitative RT-PCR, respectively. For mRNA stability assay, the total RNAs were

extracted after actinomycin D treatment at an indicated time point and submitted to quantitative RT-PCR assay. Translation efficiency was expressed as the abundance ratio of mRNA in the polysomal RNA versus the total RNA. Data are presented as mean ± standard deviation (n = 3). Asterisks indicate significant differences (*P < 0.05, **P < 0.01, ***P < 0.001; Student's t test). NS, no significance.

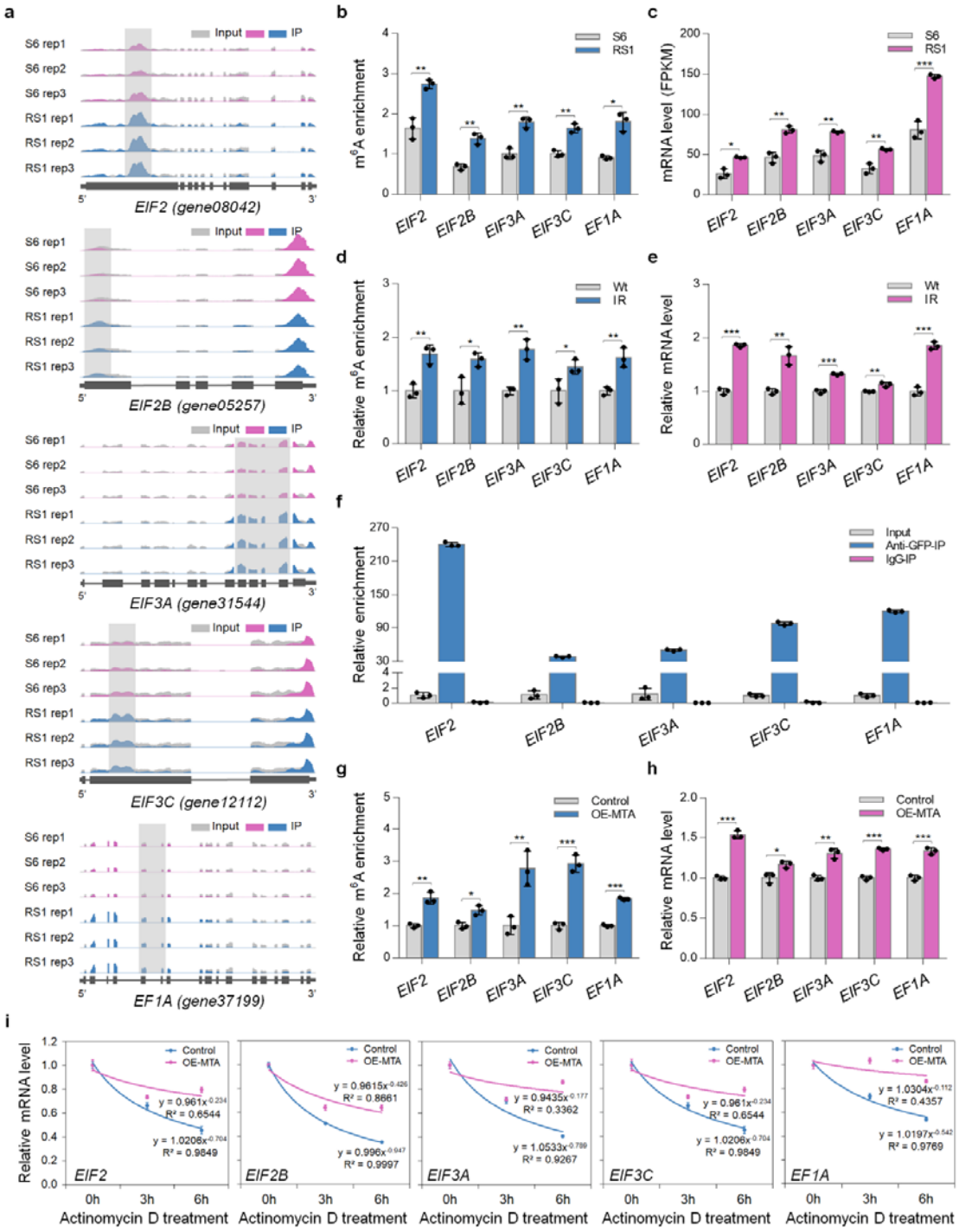

Figure 7 Influence of m^{6}A on translation initiation factors or elongation factors in strawberry. a Integrated Genome Browser (IGB) tracks displaying the distribution of m^{6}A reads in transcripts of genes encoding translation initiation factors (*EIF2*, *EIF2B*, *EIF3A*, and *EIF3C*) and elongation factors (*EF1A*). The hypermethylated m^{6}A peaks (fold change ≥ 1.5; *P* value < 0.05) in fruit at RS1 stage compared to those at S6 stage are indicated by shadow boxes. S6, the growth stage 6; RS1, the ripening stage 1. Rep, replicate. **b** m^{6}A enrichment for *EIF2*, *EIF2B*, *EIF3A*, *EIF3C*, and *EF1A* from

m^{6}A-seq data. **c** Transcript levels of *EIF2*, *EIF2B*, *EIF3A*, *EIF3C*, and *EF1A* determined by RNA-seq. FPKM, fragments per kilobase of exon per million mapped fragments. **d** and **e** Relative m^{6}A enrichment (**d**) and gene expression (**e**) for *EIF2*, *EIF2B*, *EIF3A*, *EIF3C*, and *EF1A* in the octoploid strawberry fruit at the white (Wt) and initial red (IR) stages. The relative m^{6}A enrichment and gene expression were determined by m^{6}A-IP-qPCR and quantitative RT-PCR, respectively. The *ACTIN* gene served as an internal control. **f** RNA immunoprecipitation (RIP) assay revealing the binding of MTA protein to the transcripts of *EIF2*, *EIF2B*, *EIF3A*, *EIF3C*, and *EF1A*. **g**-**i** The changes in relative m^{6}A enrichment (**g**), gene expression (**h**), and mRNA stability (**i**), of *EIF2*, *EIF2B*, *EIF3A*, *EIF3C*, and *EF1A* in the MTA-overexpressed fruits. For mRNA stability assay, the total RNAs were extracted after actinomycin D treatment at an indicated time point and subjected to quantitative RT-PCR assay. Data are presented as mean ± standard deviation (n = 3). Asterisks indicate significant differences (*P < 0.05, **P < 0.01, ***P < 0.001; Student's t test).